Variable Control of DNA Nanostructures

Undergraduate Thesis

Presented in Partial Fulfillment of the Requirements for Graduation with Undergraduate Honors in Engineering with Honors Research Distinction in Chemical Engineering at The Ohio State University

By

Michael Gustav Lindell III, B.S.

Undergraduate Program in Chemical Engineering

The Ohio State University

2016

Thesis Committee

Dr. Carlos Castro, Advisor

Dr. Lisa Hall, Thesis Committee

Alexander Marras, Graduate Mentor

Abstract

Structural DNA nanotechnology is a promising approach for the fabrication of precise nanostructures with potential applications in drug delivery, disease detection, and templating or active assembly of nanoscale components. Current research has largely focused on static DNA nanostructures. To expand functional scope, the Nanoengineering and Biodesign Laboratory (NBL) is using a technique called DNA origami to develop nanoscale machinery with designed mechanical motion and establishing methods to control their behavior. This work focuses on controlling the dynamic behavior of DNA nanohinges by changing ionic conditions in solution. We modify the hinge design by adding additional single-stranded DNA overhangs on both arms that can close the hinge in the presence of a desired solution. Results consistently showed that hinges with complementary DNA overhangs closed more readily as solution ion concentration increased, with sensitivity to hinge stiffness, length of overhangs, number of overhang connections, and location of overhangs. We also designed and fabricated an oscillator hinge for the incorporation of two-way actuation mechanisms. These findings suggest that dynamic DNA nanostructures can be designed to interact predictably with a given ionic environment based on modified structural properties. Future experiments will include the further study of overhang spatial distribution and expansion of hinge actuation studies to real-time fluorescence trials. The oscillator hinge will be used for possible theranostic applications as well as for signal propagation through polymerized chains.

Dedication

To the all-powerful and all-loving God, who both created this complex world and loves us enough to let us discover more and more of Him in it.

Acknowledgements

First and foremost, I would like to recognize and express my sincerest gratitude to my faculty advisor, Dr. Carlos Castro, and my graduate mentor, Alex Marras, for not just their foundation and support of this project, but for the many years of guidance and commitment to my growth as an engineer. If not for their leadership and example, I would know nothing of both the enjoyment found in and the perseverance necessary for the high-level research in which they both excel.

I would also like to thank my thesis committee faculty member, Dr. Lisa Hall, for her willingness to dedicate time and energy in serving on this committee. Dr. Hall is an excellent model for her students and deserves the utmost respect as a researcher and professor.

It is also necessary for me to acknowledge and thank the entire Nanoengineering and Biodesign Laboratory team, past and present, for creating and sustaining an enjoyable and supportive environment conducive to research.

Finally, I must sincerely thank my fiancé and soon-to-be wife, Sarah Folk, for the hours upon hours she has spent by my side as I pressed onward with this work. You're a saint, Sare, and none of this would have been possible without your constant encouragement.

Vita

June 2012……..Olentangy Orange High School

December 2016……B.S. Chemical Engineering, The Ohio State University

Fields of Study

Major Field: Chemical Engineering

Specialization: Biomolecular Engineering

Minor Field: Spanish

Table of Contents

List of Tables

Table of Figures

Chapter 1: Introduction

1.1 Nanoscience and Nanotechnology

Many of the world's unanswered questions are no longer about the things we might see, but more about the things unseen and often unimaginable. Billions of dollars every year are spent in efforts to fight diseases like coronary heart disease, cancer, chronic lower respiratory disease, and the countless others that account for more than two million deaths per year in the U.S alone [1]. New materials and production processes are constantly being developed in order to improve everything from impact strength of cars to shelf-life of common grocery items. Alternative energy, a highly relevant topic for environmentally-conscious investors and engineers for the past several decades, has seen a growing focus on hyper-efficient solar cells, chemical additions for fossil fuels, and enhanced turbine and rotor materials [2]. A common thread that connects all of these research and development frontiers is the need not for bigger and better, but smaller and more efficient. Making things better and more efficient often requires controlling the constituent materials and components down to the molecular scale. This need along with the development of methods to manipulate, control, and observe material and components at previously inaccessible small length scales has given rise to the field of nanoscience and nanotechnology.

Nanoscience is the science, engineering, and technology that is conducted at the nanoscale, which is typically defined as the range of 1 to 100 nanometers. On a comparative scale, if a marble were a nanometer, one meter would be the size of the Earth [3]. Often difficult to put into perspective, the incredibly small scale in which nanoparticles exist was, for many years, largely impossible to work with due to technology limitations in synthesis and imaging. Often referred to as the foreshadowing of nanotechnology, the field's origins are attributed to physicist Richard Feynman, who in 1959 gave a lecture titled "There's Plenty of Room at the Bottom" that suggested the possibility of building machines small enough to manufacture objects with atomic precision [4]. Since then, the field of nanotechnology has exponentially grown in prominence and application. Pharmaceuticals and medical treatments are improved with the help of nanoparticles that aid in drug delivery

and disease detection [5] [6] [7]. Manufacturing materials have been enhanced with nanoparticles to increase strength, insulation, conductivity, and many other desired functions, and the energy field has exploded with the impact of nanotechnology in the improvement of solar cells and natural resource harvesting techniques [8] [9] [10]. Though small by definition, the field of nanotechnology seems to be endlessly expanding to solve major issues in the world and press into some of the most innovative research ever conducted.

Specifically relevant for this work, nanotechnology has a far-reaching potential for applications in the human body. Applications include, but are certainly not limited to, targeted drug delivery, bioassays, disease detection, mechanical characterization of body processes, and structural manipulation of cellular constructs. In this subfield of bionanotechnology, one of the greatest obstacles is now creating nanomaterials that can be incorporated successfully into a living body (*in vivo*). When nanoparticles are used *in vivo*, there is always a risk that the body will naturally fight back against the foreign object, or that the nanoparticle is created from materials that can have detrimental toxic effects on cell tissue [11]. For this reason, recent efforts have been largely focused on the utilization of naturally-occurring materials in the body to create nanostructures that can function while not being recognized as non-foreign agents [12]. Finally we arrive at the growing interest in, and need for, DNA nanotechnology.

1.2 Introduction to DNA Origami

Deoxyribonucleic Acid (DNA) is well-known as the fundamental genetic material found in almost every living organism. While its base-pairing properties allow it to store genetic information for biological processes, DNA has more recently been used in the nanotechnology field for its unique mechanical properties [13] [14] [15] [16] [17]. Many intrinsic properties of DNA are exploited in order to construct complex structures in a relatively new field of bionanotechnology—structural DNA nanotechnology.

The molecular structure of DNA, composed of nitrogenous bases, five-carbon sugars, and phosphate groups, is a twisted ladder-like geometry known as the DNA double helix. The rungs of this ladder are formed by nucleotide bases adenine (A), thymine (T), cytosine (C), and guanine (G). The legs of the ladder are sugar-phosphate backbones that link the

bases of the DNA molecule together along the length of the helix. Nucleotide bases are connected by hydrogen bonds in a specific manner, where base pairs bind according to Watson-Crick base-pairing rules—adenine binds with thymine (A-T) and cytosine with guanine (C-G) [18]. As depicted in Figure 1, this base-pair binding specificity is due to the structures of the nitrogenous bases, where cytosine and guanine both have three H-bond sites, but adenine and thymine only have two, a property that also makes C-G bonds stronger than A-T [19].

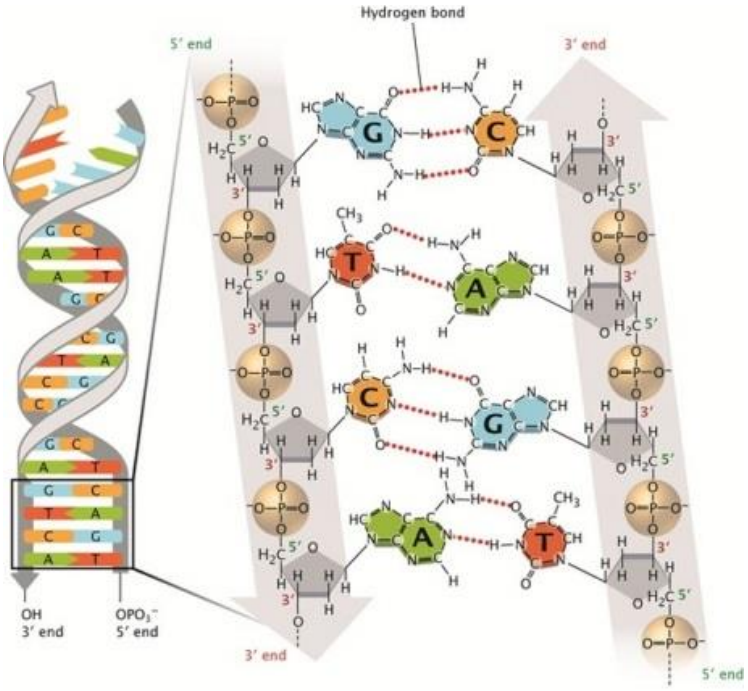

Figure 1: DNA consists of a sugar-phosphate backbone and nucleotide bases Adenine, Thymine, Guanine, and Cytosine. The specific hydrogen bonding of these bases is what cause single-stranded DNA to form double helices [20].

The specific self-assembly properties and intermolecular interactions of DNA are utilized in the design and fabrication of DNA nanostructures. A relatively young field, the first publication conceiving a structural use for DNA came out in the early 1980's by Nadrian Seeman [13]. Here, Seeman proposed the ability to pair ssDNA strands to form immobile junctions that could be organized into arrays to form lattices. This seminal work established the foundation for DNA nanotechnology. Within a few years, the first DNA cubes were produced by Seeman and co-workers [21]. Since then, the field has rapidly evolved into

utilizing the elementary principles of Watson-Crick base-pair binding to create 2D and 3D structures capable of being formed with high precision and yield. Figure 2, a graph of citations in DNA nanotechnology research every year, shows how the field continues to grow today, introducing a variety of shapes and functions of self-assembling DNA nanostructures that are used in applications including bio-assays, drug delivery, mechanical manipulation, and much more [22] [23].

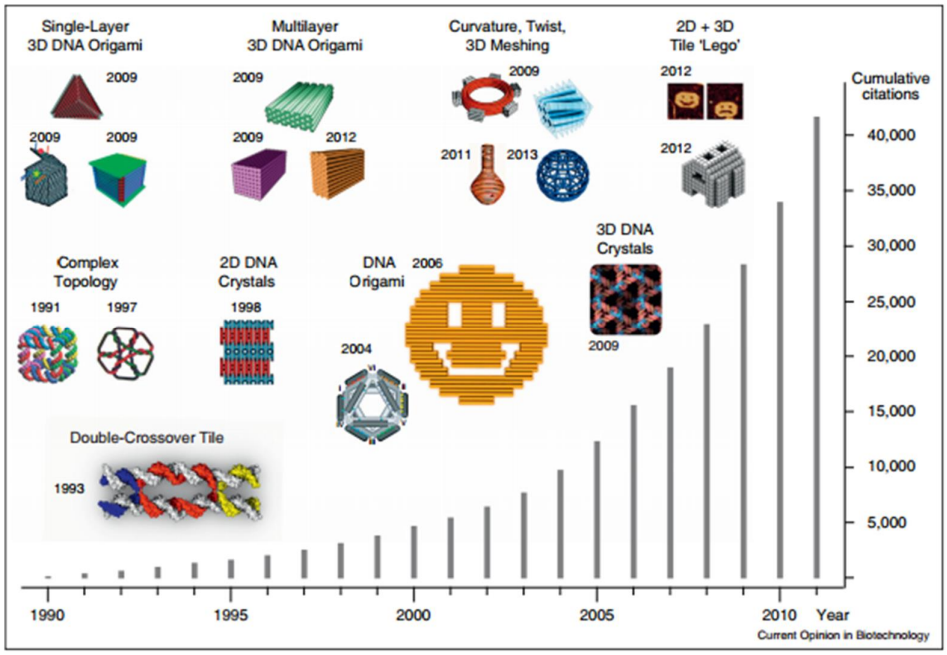

Figure 2: The relevance and importance of DNA nanotechnology has increased exponentially since its inception in the late 1980's [15].

DNA origami, a particularly successful approach to creating custom, discrete objects at the nanometer scale, has gained popularity since its introduction in 2006 [14]. This technique involves adding many ~30-50 base single-stranded DNA (ssDNA) oligomers to a long, ~7000-8000 base circular ssDNA scaffold such that the oligomers bind to the scaffold in a specific, piece-wise manner. The specific binding of ~100-200 staple strands to the scaffold in this technique allows for compact geometries to be created with a high level of precision, as can be seen in Figure 3: DNA origami is a nanotechnology that utilizes the self-assembly of ssDNA to fold functional nanostructures. A ssDNA scaffold of ~7000-8000 bases binds to ssDNA staple strands that are partially complementary to specific sections of the scaffold.

Figure 3. Typically, the scaffold is derived from the single-stranded M13mp18 bacteriophage genome, and staples are synthesized to be piecewise complementary to the scaffold [24]. In reference to macroscale mechanical structures, double-stranded DNA (dsDNA) helices and bundles of dsDNA helices act like stiff cylinders while ssDNA are comparable to flexible cables. The bottom-up nature of the DNA origami structure self-assembly, along with the ability to add functional groups to binding staples, allows the design and construction of an almost endless variety of nanostructures capable of interacting with many different environments and molecules. More on the design and assembly of scaffolded DNA origami structures can be found in CH. 2 – DNA Origami Fabrication Methodology. This project focusses on the manipulation of dynamic DNA nanostructures based on environmental and design-specific factors.

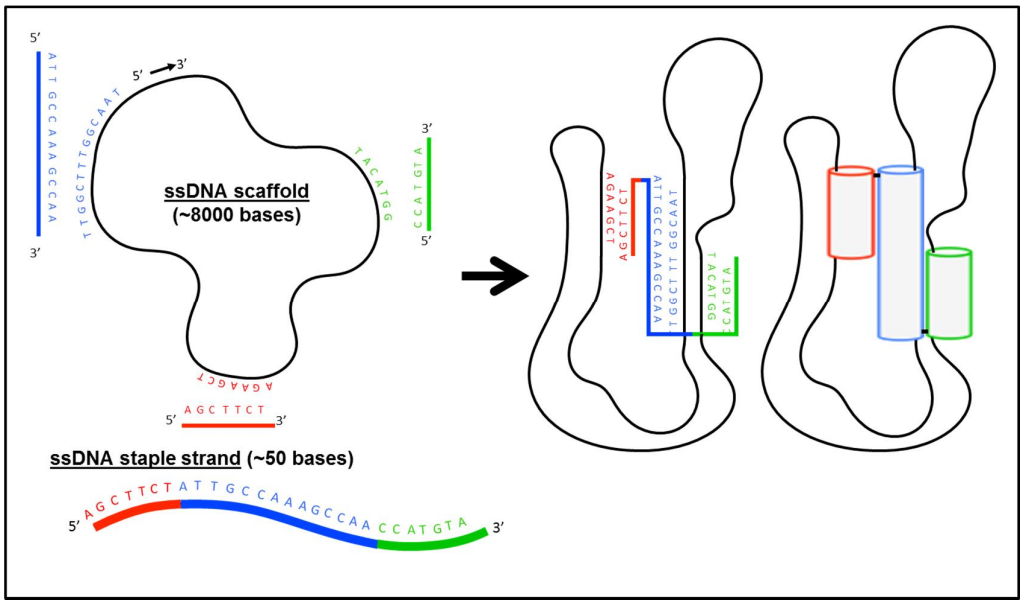

Figure 3: DNA origami is a nanotechnology that utilizes the self-assembly of ssDNA to fold functional nanostructures. A ssDNA scaffold of ~7000-8000 bases binds to ssDNA staple strands that are partially complementary to specific sections of the scaffold.

1.3 Existing Technologies and Limitations

With the field of scaffolded DNA origami rapidly expanding, many new applications are continuously being developed with novel nanostructures. Soon after the first DNA origami structures were fabricated by Rothemund's group in 2006, static 3D architectures were successfully created by William Shih and co-workers in 2009 [25], who also developed the

first twisted and curved geometries in the same year [26]. More recent innovations have led to the leap from static nanostructures to dynamic nanomachines, which have become the current focus of the field for their more extensive applications.

Dynamic and reconfigurable scaffolded DNA origami is now finding uses in many areas, including biosensing, drug delivery, mechanical manipulation, bioassays, and much more [17] [27]. Functional groups, including ligands and aptamers, can be selectively placed on structure surfaces for user-defined functions as biomaterials [28]. Position-controlled attachment of nanomaterials to origami structures has been employed for increased functionality of gold nanoparticles (AuNPs), organic dyes, and quantum dots [29] [30]. Biological structure determination and imaging capabilities have been improved through the incorporation of tubular and crystalline DNA [31] [32]. Biosensing and beacon DNA nanostructures have been used for the target of specific proteins and genes [33] [34]. Biological and molecular payloads can be transported and distributed via DNA origami structures [22] [35]. Synthetic lipid-membrane channels can be formed by DNA nanostructures [36]. Figure 4 shows many examples of existing DNA origami structures.

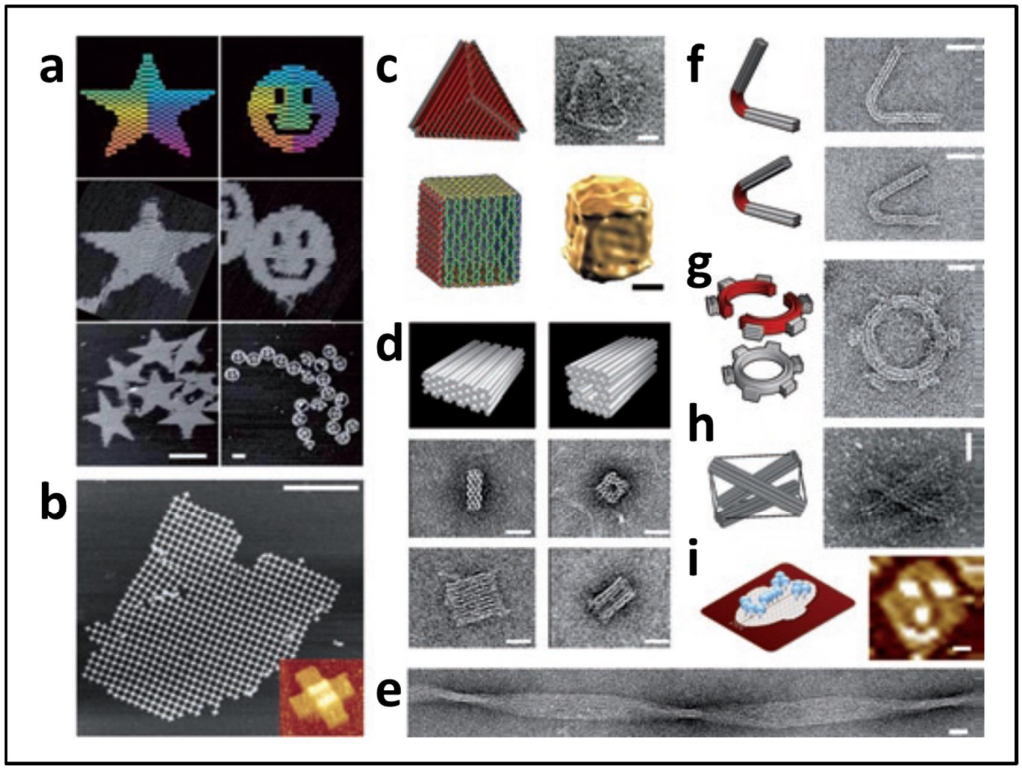

Figure 4: Examples of objects built with scaffolded DNA origami include [24]: (a) Designs of single-layer DNA origami shapes (top) and AFM images of these objects (middle and bottom). The pointed star and the smiley face each have diameters of ~100 nm [14]. (b) AFM image of crystalline DNA origami arrays formed from several hundred copies of a cross-shaped single-layer DNA origami object. Inset, image of a 100-nm-long cross-shaped origami monomer [37]. (c) Container-like DNA origami objects (left) imaged with negative stain TEM (top) and cryogenic TEM (bottom) [38]. (d) Design and images of multilayer DNA origami objects [25]. (e) Image of a multimeric multilayer DNA origami object with global twist deformation [26]. (f,g) Design and images of space-filling multilayer DNA origami objects such as bent bars (f) and a gear with square teeth (g) displaying custom curvature [26]. (h) Tensegrity prism created by combining multilayer DNA origami struts and ssDNA strings [39]. (i) Design and image of a single-layer DNA origami shape with site-directed protein attachments [40]. Scale bars, 100 nm (a), 1,000 nm (b) and 20 nm (c–i).

Most directly influencing our work are the reconfigurable DNA origami structures that utilize strand displacement [41] for changes in structural conformation. A strand with the highest binding affinity to another strand that is already bound in a Watson-Crick base-pairing double helix will displace and replace the lower affinity ssDNA. The ability to displace specific DNA strands can be used to induce a conformational change in a DNA origami structure [34] [42] [17]. Specifically, the work done by target ssDNA strands to bind to ssDNA overhangs on a Bennett Linkage structure, fabricated by Alex Marras in the NBL, trigger the closing and opening of this structure into and out of higher energy states [43]. This strand-

based actuation mechanism, which will be discussed later in its applications for this work, can be seen in Figure 5.

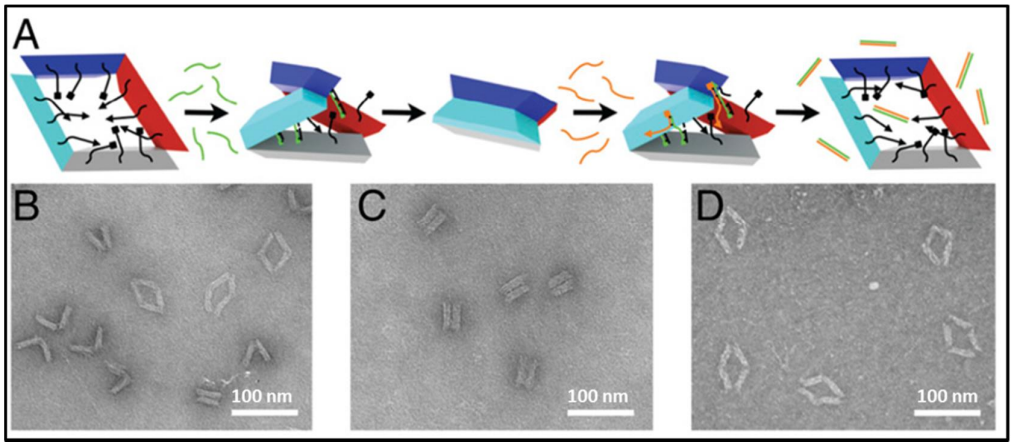

Figure 5: The Bennett linkage DNA origami structure, originally fabricated by Alex Marras in the NBL, was shown to be actuated in the presence of specific target ssDNA strands. A) Schematic of the closing and opening of the Bennett linkage. B-D) TEM images corresponding to different structural conformations. Modified from [43].

While new and innovative DNA nanostructures are being produced at a rapid pace, there still exist many limitations and obstacles to overcome in the field, particularly in relation to the integration of multiple functions in a single device, research into the fundamental molecular processes and physics behind DNA nanotechnology, cost reduction for scale-up, and applications *in vivo* [15] [44]. Nonetheless, the field of DNA nanotechnology, and more specifically scaffolded DNA origami, presents an exciting future outlook that will undoubtedly aid in the discovery of solutions to some of the world's greatest needs.

1.4 Thesis Objective and Overview

While the design and fabrication of many innovative DNA nanostructures is currently being accomplished in many labs, it is imperative that we gain a much more in-depth understanding of the mechanisms used to manipulate these structures so that highly functional devices ready for successful use in a number of fields can be created. The objective of this thesis is to better understand the function and to develop new actuation capabilities for dynamic DNA origami devices by studying the effect of various design

parameters on the behavior of a DNA origami hinge in ion-rich environments. The characterization of these nanostructures could lead to more intricate and elegant solutions to current questions in drug delivery, nanomanufacturing, and biophysical assays.

This thesis includes five chapters. Chapter 1—Introduction aims to provide a relevant scope and necessary knowledge base about DNA nanotechnology and DNA origami. Chapter 2—DNA Origami Fabrication Methodology outlines the general process for designing, creating, purifying, and analyzing DNA origami structures and provides information on the fabrication of the studied nanohinge. Chapter 3—Hinge Angle and Actuation Characterization covers all of the results from several standard and modified hinge studies, and Chapter 4—Oscillator Hinge explains the next-generation dual hinge design and preliminary results. Finally, Chapter 5—Conclusion is a summary of the whole thesis and future directions.

Chapter 2: DNA Origami Fabrication Methodology

2.1 caDNAno Design

The first step in DNA origami fabrication is determining how to design the binding between ssDNA scaffold and staples in a manner that will maximize base pairing in the desired geometry. In this step, the scaffold must be routed into the custom design through modeling the basic geometry with cylinders, then staples are paired to the scaffold. For any given design, there are countless staple lengths and binding conformations that could be used to produce a geometry, but the way in which staples cross over between points on the scaffold effects the stiffness and strength of the structure [44], as well as the overall folding yield and rate of assembly. However, the details of how design parameters affect the folding process are not currently well-understood.

caDNAno has emerged as a well-established software in the field for DNA origami design [45]. This open-source software allows a user to diagram single and multilayer DNA origami objects in either honeycomb or square lattice packing [25] [24] [46]. Good practice of caDNAno design utilizes color-coded groups of staples to separate modulus or components within a design or simply to better visualize major sections of a structure [24]. The 3D structure of a caDNAno design can be predicted using the computational framework CanDo, which also predicts mechanical stresses and double-helix curvature [24] [47]. Figure 6 shows several designs in caDNAno, CanDo, and then as final products viewed using Transmission Electron Microscopy (TEM).

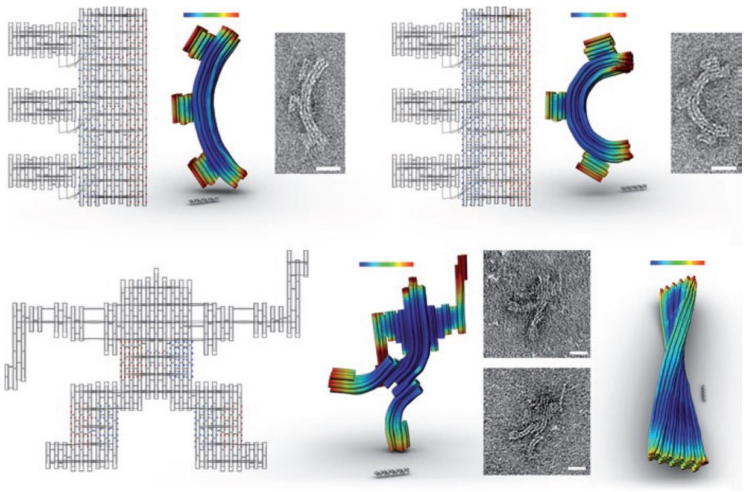

Figure 6: 3D computational softwares caDNAno and CanDo aid in the design of scaffolded DNA origami structures [24].

2.2 Folding Reaction and Purification

The typical workflow and protocol details for the fabrication of DNA origami structures is described in "A primer to scaffolded DNA origami" [24]. An overview is provided here. After the design stage, scaffold of a specific length derived from the M13mp18 ssDNA genome is combined with design-specific staples in five to ten-fold excess and placed in an ion-rich aqueous buffer. This solution is then subjected to a thermal denaturation and annealing procedure to facilitate self-assembly, in which the temperature is raised high enough to denature any existing dsDNA (65-80°C), then slowly lowered to allow binding of staples to the scaffold. Typically longer staples will bind to the scaffold at higher temperatures, so it is important when assigning staple connections to place larger staples on inside locations of any structure. Once the thermal ramp process has finished, solutions containing a mixture of well-folded structures, misfolded structures, and excess staples should be purified through either agarose gel electrophoresis or via centrifugal purification with 15% polyethylene glycol (PEG) 8000 [48]. The structures extracted from these purification processes are ready for imaging and analysis.

For all DNA origami structures discussed in this paper, a variant of the M13Mp18 circular ssDNA genome was used as the scaffold [25] (7560 bases for Hinge 1, 8064 bases for Hinge 2 and the oscillator hinge) and combined with commercially-ordered staples (Eurofins Genomics) in 10x excess. The scaffold and staples were placed (concentrations of 20 nm and

200 nm respectively) in a folding buffer containing 5 mM Tris, 1 mM EDTA (TE), NaCl and $MgCl_2$ at a concentration specific to the structure and trial, and double-distilled water (ddH_2O).

Two temperature ramps were utilized throughout the many different experiments conducted in this work. The primary, and most established, thermal ramp used for structure self-assembly spanned 2.5 days, and consisted of a rapid heating to 65°C followed by slow cooling to 4°C. The second ramp, which we refer to as a "rapid fold," consists of holding the reactants at a constant temperature for several hours. This technique has been previously validated [49], and encourages the rapid production of DNA nanostructures at the same yield and in significantly less time than the traditional annealing process. The rapid fold used for all structures discussed in this paper spanned only 4.5 hours, and the annealing temperature was determined by screening several annealing temperatures exploiting the temperature gradient function of the thermocycler heating block.

Purification via PEG was used for angular distribution trials discussed in section 3.2 of this paper. In this process, product from the folding reaction was combined in equal volume with a solution containing 15% PEG 8000 dissolved in ddH_2O and centrifuged for 30 minutes at 16,000 g at 4°C. PEG polymers promote pelleting of the relatively large DNA origami structures and enable removal of excess staples from the folded structure in solution [48], which are extracted with the supernatant. The pellet of DNA origami structures can then be resuspended in an experimental buffer.

Agarose gel electrophoresis was used to purify most structures discussed in this paper. The gel was made up of 2% agarose in the presence of 0.5x TBE, EtBr, and 11 mM $MgCl_2$. The gels were run at 70V for 3-4 hours to allow time for structures to completely separate [24]. Images of finished gels were taken under UV light to observe bands of purified structures, an example of which can be found in Figure 7. Well-folded structures usually run at around the same speed as the source scaffold, and are excised upon completion of the purification step for resuspension in solution and imaging via TEM.

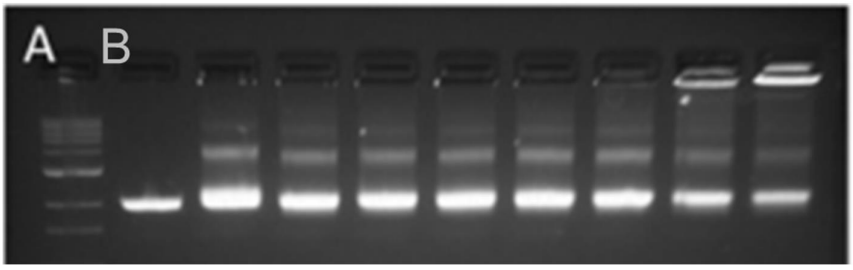

Figure 7: Sample image of a finished agarose gel after electrophoresis. Typically, structures are run alongside A) a ladder for normalization reference to other gels and B) a blank scaffold. Eight duplicate lanes were run in this gel to show consistency.

2.3 TEM Imaging and ImageJ

TEM is commonly used to view nanostructures in a fixed conformation. Products of the gel electrophoresis were placed on copper mesh grids with a carbon film and negatively stained with 2% uranyl formate (UFo) in preparation for imaging [24]. Finally, nanostructures were imaged on a Tecnai G2 bioTWIN TEM at an electron acceleration voltage of 80 kV.

For the entire hinge angle characterization work discussed later, the ability to measure the angle of hinges in TEM images was necessary. The software ImageJ was used for these angle measurements. This program allows the user to select three points on an image, and calculate the angle between these points (see Figure 8). While user error could cause discrepancies in angle measurements, it is important to note that hinge angle measurements were not significantly different in a test of user variability between myself and Alex Marras.

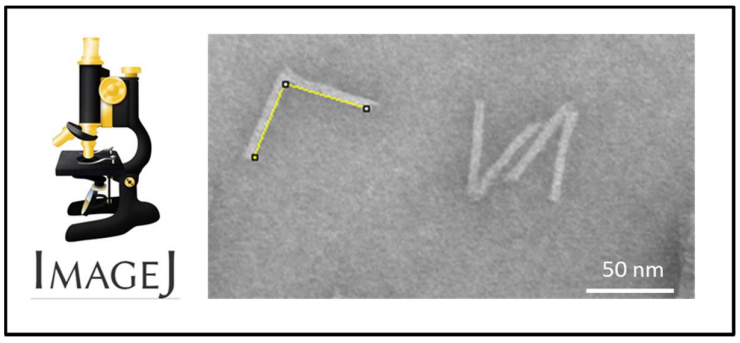

Figure 8: ImageJ allows users to calculate hinge angles from TEM images.

Chapter 3: Hinge Angle and Actuation Characterization

3.1 Design

The focus of this thesis is on the manipulation of a novel nanohinge recently developed in the Nanoengineering and Biodesign Lab [43]. The basic hinge model consists of two stiff bundles of 18 dsDNA helices attached by six ssDNA connections. The six connecting strands, which are sections of the scaffold, are comprised of three short loops and three long loops, as can be seen in Figure 9. The nanohinge mimics the motion of a macroscale hinge, where the two arms are free to swing open and closed and are constrained to a single rotational degree of freedom.

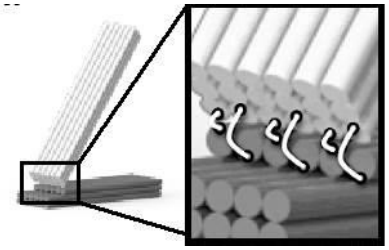

Figure 9: Six ssDNA connections form the vertex of the DNA origami hinge, with variable lengths between Hinge 1 and Hinge 2 [43].

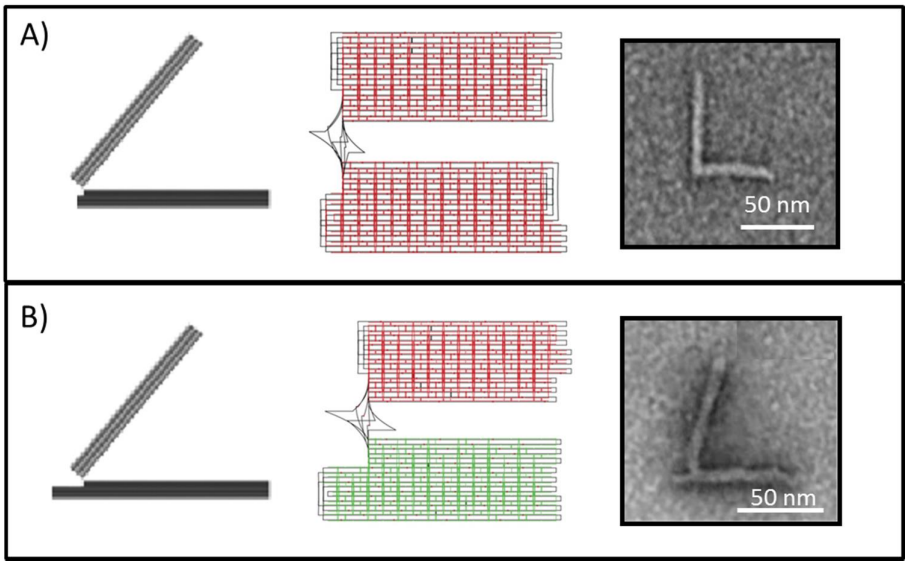

Figure 10: Two versions of the DNA origami nanohinge were created: A) Hinge 1 and B) Hinge 2. The hinge was originally created by Alex Marras in the NBL.

Two versions of the hinge were created in order to study the effect of hinge torsional stiffness on the motion of the hinge arms, as is depicted in Figure 10. The first version, Hinge 1, was created using a 7560 base scaffold, and has short connections of two bases and long connections of 16 bases. Hinge 2, created using an 8064 base scaffold, also has short connections of 2 bases, but differs from Hinge 1 with long connections of 30 bases and is inhibited at high angles by an extension of the bottom arm that impedes opening of the hinge. The hinge, due to its flexible yet strong connection strands, acts as a torsional spring. Because Hinge 1 has shorter connection strands than Hinge 2, it is torsionally stiffer, and in particular, less likely to fluctuate to small angles. Figure 11 displays the calculated energy landscapes of the two hinges [43]. Energy landscapes show the changes in energy at different structural conformations, where lower Free Energy (k_BT) signifies a higher probability of a hinge being found at that angle. The free-energy landscapes U(θ) of these hinges were calculated using Equation 1 and Equation 2, where P(θ) is the probability distribution of hinge angles, k_B is Boltzmann's constant, T is absolute temperature, and Z is the partition function. From the energy landscapes it can be observed that Hinge 2 prefers to be at lower angles than Hinge 1.

Equation 1: Probability distribution

$$P(\theta) = \frac{\exp\left(-\frac{U(\theta)}{k_B T}\right)}{Z}$$

Equation 2: Free-energy landscape

$$U(\theta) = -k_b T ln\{P(\theta)\} - k_B T ln(Z)$$

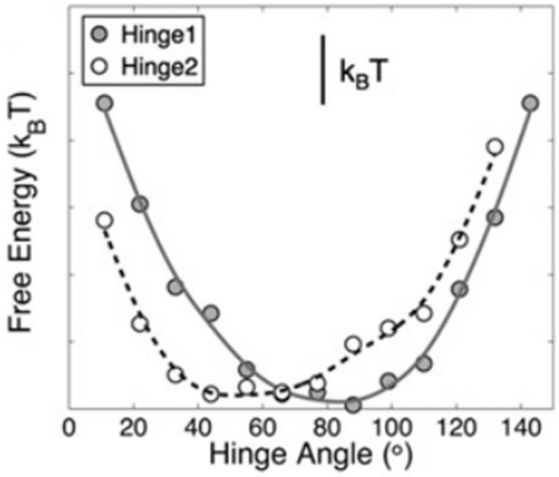

Figure 11: The energy landscapes of the two hinge designs show that Hinge 1 prefers higher angles than Hinge 2 [43].

As is discussed later, the basic hinge can be modified in a number of ways in order to give it specific functionality. Most of the possible functionality of a hinge, whether in drug detection/delivery or mechanical manipulation, comes from the fact that it is either fully open, fully closed, or at some angle in between. There exist many possible factors that could change the angle or conformation of a hinge in a given solution. Since we are interested in using ions to actuate the structure, here we tested the effect of varying concentrations of monovalent, NaCl, and divalent, $MgCl_2$, cations on the conformational distributions and energy landscapes of the hinge.

3.2 NaCl vs. $MgCl_2$

It is well known than in order to stabilize negatively-charged DNA nanostructures, they must be suspended in buffers of positively-charged cations that will screen interhelical repulsion. While for many years it was believed that divalent cations (like Mg^{2+}) were necessary for stable structures, it was recently shown that monovalent cations (like Na^{+}) can also be used in salt buffers to stabilize DNA origami structures [50]. Much work in the DNA origami field is directed towards future applications *in vivo*. In order to make useful characterizations of the hinge so that it could one day be used in the human body, we

decided to study the effect on hinges of two highly abundant ions: sodium and magnesium. The objective for this study was two-fold: first, we wanted to understand how hinge dynamics are affected by changes in ion concentration, and second, whether hinge behavior is different in sodium-rich or magnesium-rich solutions. All hinge trials for this angle characterization study were performed using the Hinge 1 design.

Initial screens of salt conditions for folding revealed optimal folding in 1.2 M NaCl or 20 mM $MgCl_2$. For the sodium trials, hinges were folded in 1.2 M NaCl, PEG purified, and resuspended in 0.2 M, 0.6 M, 1 M, 1.2 M, or 1.4 M NaCl buffers. For magnesium trials, hinges were folded in 20 mM $MgCl_2$, PEG purified, and resuspended in 5 mM, 10 mM, 15 mM, 20 mM, 25 mM, or 40 mM $MgCl_2$ buffers. These ion concentrations were chosen based on the knowledge that DNA origami becomes unstable at very low or aggregates at relatively higher concentrations of salt [50] [51]. Images were then acquired using a TEM, and hinge angles were manually measured using ImageJ. During the grid preparation step for TEM imaging, the sodium trial hinges were treated with a magnesium buffer wash between structure deposition and staining in order to improve staining quality. This wash was performed by applying hinge solution to a grid, allowing for hinges to settle and stick to the grid, then removing the solution with filter paper and subsequently dotting the grid with 10 µL of 0.5x TBE with 11 mM $MgCl_2$ solution. This magnesium solution was wicked away immediately, and did not appear to have any effect on the hinge angles. A minimum sample size of 200 measurements was recorded at each ion concentration.

Figure 12 shows the results of the hinge angle measurements in sodium and magnesium solutions. In the magnesium trials, hinges preferred to be at an angle of 60°-80° for all experimental ion concentrations. The energy landscapes did not change as ion concentrations increased. In contrast, a shift in preferred angles was observed in the sodium trials. As the sodium concentration increased in solution, hinges more often adopted conformations with smaller angles. While the mean hinge angle in magnesium solution stayed consistently at 75° +/- 2 as ion concentration increased, the mean hinge angle in sodium solution dropped from 84° to 68° as the ion concentration increased from 0.2 M to 1.4 M. A summary of the mean hinge angle for each ion concentration can be found in Table 1 below.

Table 1: The mean angle for hinges in sodium-rich solutions significantly decreased with increasing ion concentrations, while the mean angle in magnesium did not significantly change with increasing ion concentration.

Na^+		Mg^{2+}	
Concentration (M)	*Mean Angle (°)*	*Concentration (mM)*	*Mean Angle (°)*
0.2	**84** +/- 26	5	**76** +/- 23
0.6	**78** +/- 23	10	**73** +/- 23
1	**76** +/- 22	15	**78** +/- 21
1.2	**69** +/- 24	20	**79** +/- 24
1.4	**68** +/- 25	25	**73** +/- 25
		40	**77** +/- 23

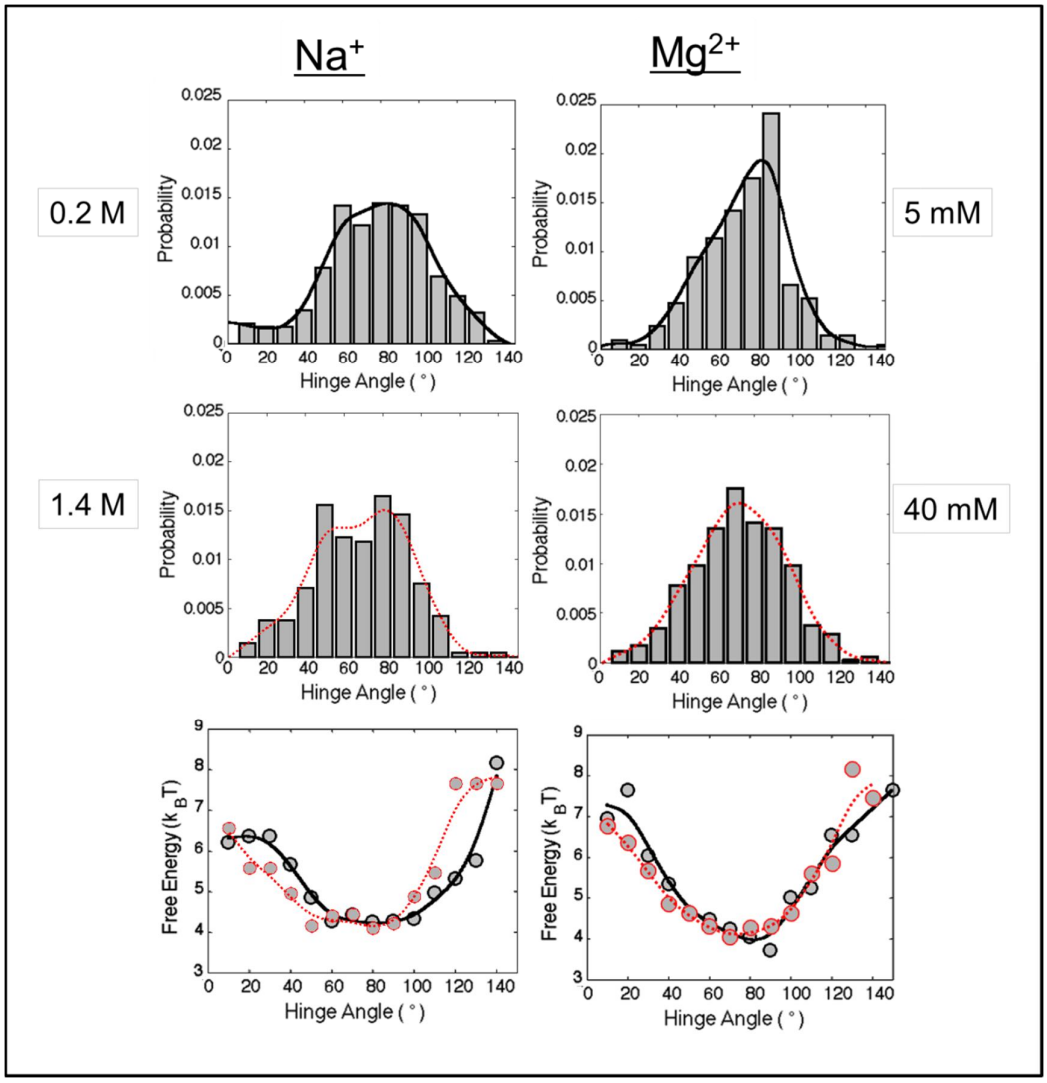

Figure 12: Hinge angle distributions and energy landscapes at minimum and maximum ion concentrations.

We concluded that changing solution magnesium concentrations in this range does not affect the angle characterization of DNA origami hinges, but changing solution sodium ion concentrations does have a slight effect on the energy landscape of these hinges. In order to avoid adverse effects on hinge conformations moving forward with functionalized hinge trials, all further tests were performed using magnesium solutions.

3.3 Ion-based Actuation

A major goal of this project was to obtain a high level of control over the opening and closing of hinges through changing only solution environment conditions. If a DNA nanostructure could automatically respond to specific factors in a given environment, it could be designed in a way that uses its actuation as a means of detecting and acting upon the presence of those environmental factors. The detection of changing ion concentrations in solution is a potential application of these DNA origami hinges.

The negative charge on DNA molecules makes the presence of positive ions essential to stabilize the formation and maintenance of base-pairing interactions, which means DNA duplex stability increases with increasing ion concentration [52]. With this in mind, a modified hinge was designed and created that could hopefully close more readily in response to increasing solution ion concentrations. This ion-based actuation would be accomplished through the binding of complementary, ssDNA overhangs on the inside faces of both hinge arms. These overhangs were designed to be weak enough so that they will not bind tightly in standard buffer conditions; but in the correct environment, these complementary overhangs should bind, which in turn would force the hinge fully closed. We hypothesized that hinges with complementary overhangs could be found in a closed conformation more frequently as solution ion concentrations increased. The general design and actuation schematic of the hinge with overhangs (HingeOH) can be found in Figure 13 below.

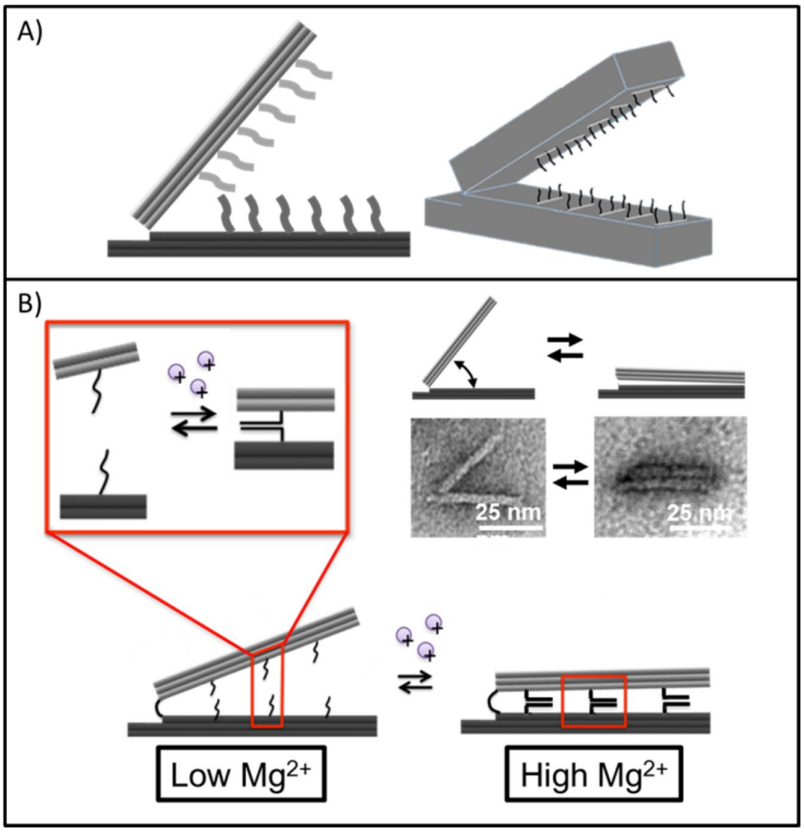

Figure 13: A) The standard DNA origami hinge was modified with the addition of ssDNA overhangs on the inside faces of both arms. Each overhang was complementary to the overhang on the opposite surface. B) Magnesium ions are essential for the stable base-pair interactions of overhangs, which cause the hinge to close.

Not only was it hypothesized that increasing ion concentrations would cause the actuation of more hinges, but we also hypothesized that the actuation of hinges could be tuned through ssDNA strength (length of overhangs) and number of overhang connections. The modified hinge was designed with several different configurations to test these hypotheses. We created hinges with overhang lengths of four, five and six bases (4b, 5b, 6b) and 10, 20 and 30 connections (10c, 20c, 30c) on each face. These different configurations are displayed in Figure 14. The first HingeOH trials were performed by modifying Hinge 1 with overhangs (H1OH).

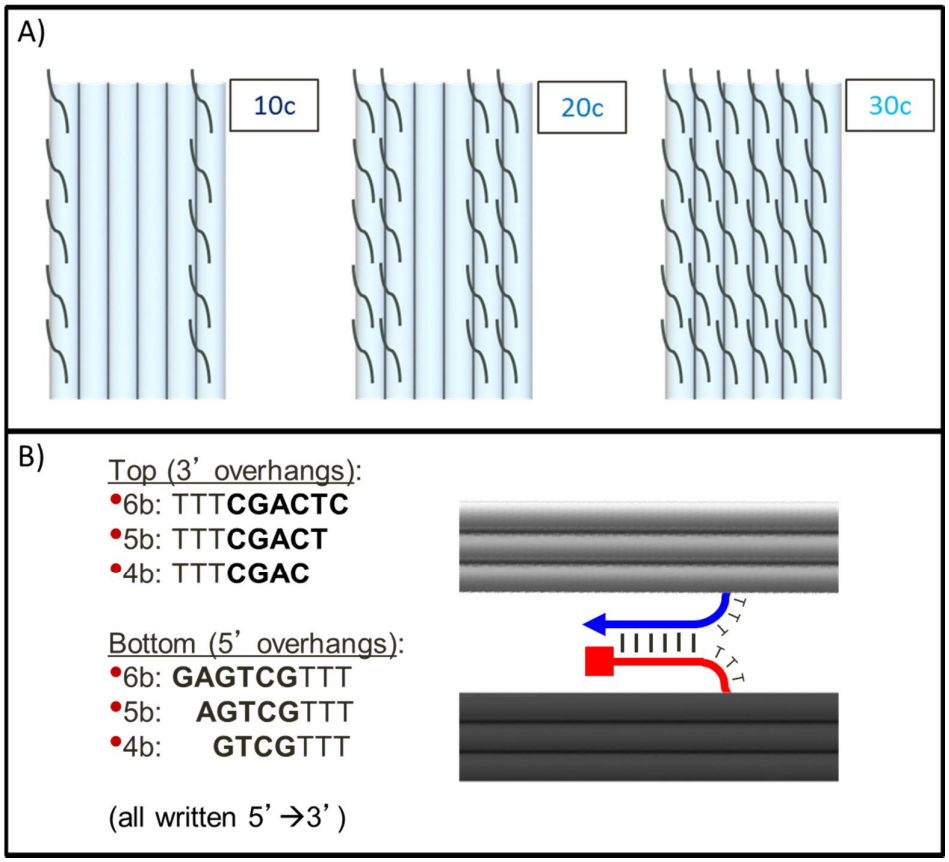

Figure 14: A) Hinges were designed with 10, 20, or 30 overhang connections on each face. B) Overhangs were either four bases, five bases, or six bases long with three thymine bases to add distance from the hinge face.

Five different H1OH designs were tested: 4b-10c, 4b-20c, 4b-30c, 5b10c, and 6b-10c. For each H1OH trial, the structures were folded in 20 mM $MgCl_2$ for either a 2.5 day annealing ramp or 4 hour rapid fold, gel purified, and resuspended in 5 mM, 20 mM, 40 mM, or 80 mM $MgCl_2$ solution. TEM images revealed large populations of well-folded hinges that exhibited either an open or closed conformation with the relative fractions depending strongly on the buffer salt conditions. A sample size of at least 200 hinges was recorded for each ion concentration and trial, and three total replicates of each measurement were performed. Sample TEM images of a few trials can be found in Figure 15. The percentage of closed hinges was calculated with using Equation 3.

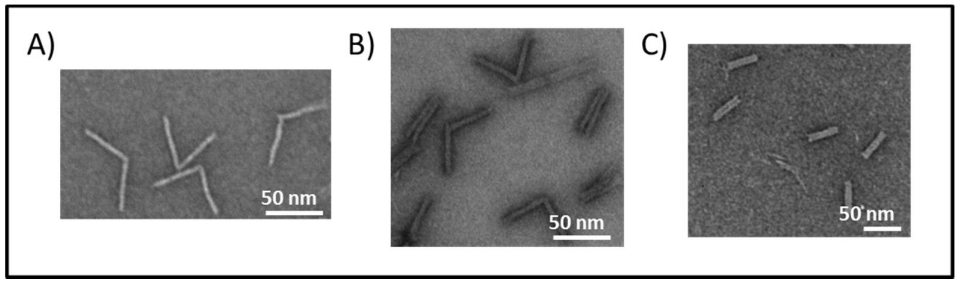

Figure 15: Sample TEM images show that hinges can be easily counted as open or closed. A) H1 4b-10c in 5 mM $MgCl_2$. B) H1 5b-10c in 20 mM $MgCl_2$. C) H1 6b-10c in 40 mM $MgCl_2$.

Equation 3: Closing percent of hinges

$$\% \, Closed = \left[(Total\ closed\ hinges) / (Total\ counted\ hinges) \right] * 100$$

Actuation curves shown in Figure 16-Figure 18 display the consistent closing nature of these modified hinges with increasing ion concentration. In Figure 16 it can be seen that the number of overhang connections has a direct effect on hinge actuation. Figure 17 shows that overhang length also directly effects hinge actuation. Finally, a summary plot can be seen in Figure 18, which shows the comprehensive actuation character of the five different overhang designs.

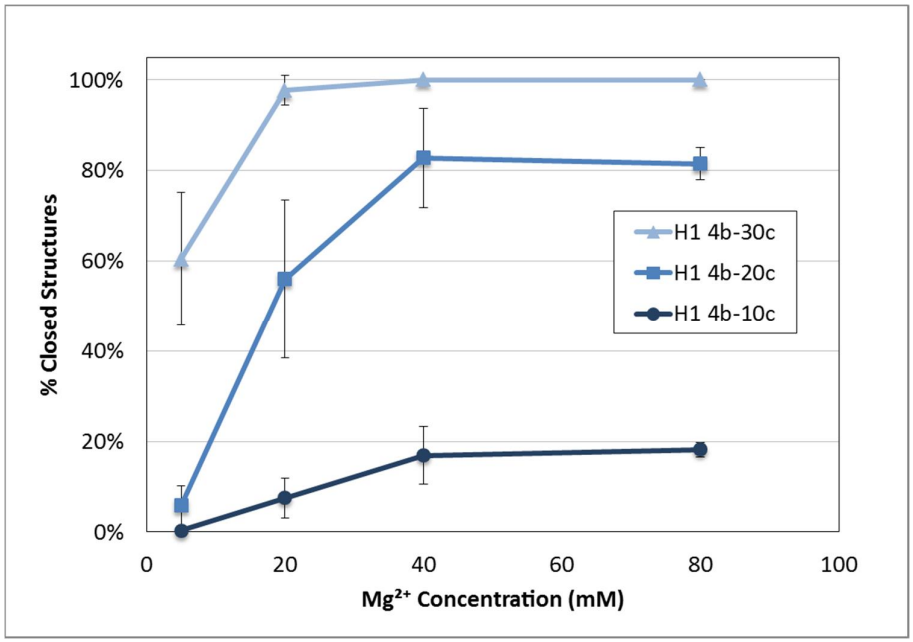

Figure 16: Actuation curves for Hinge 1 with 4-base overhangs and 10, 20 and 30 overhang connections. H1OH closes more readily with increasing number of overhang connections.

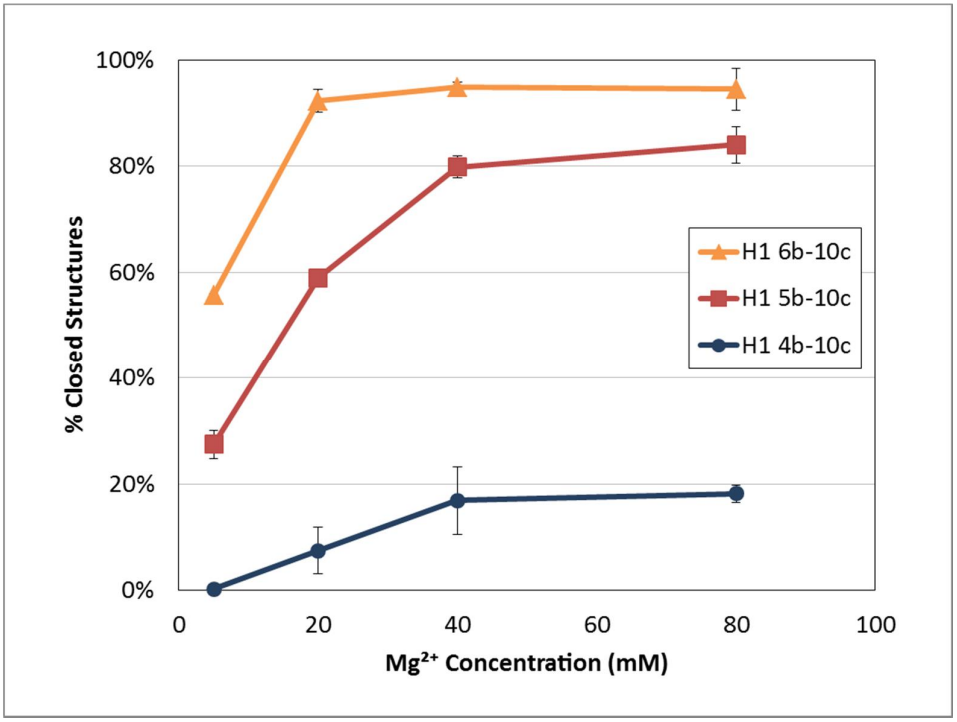

Figure 17: Actuation curves for Hinge 1 with 10 overhang connections of 4, 5, and 6 bases. H1OH closes more readily with increasing overhang length.

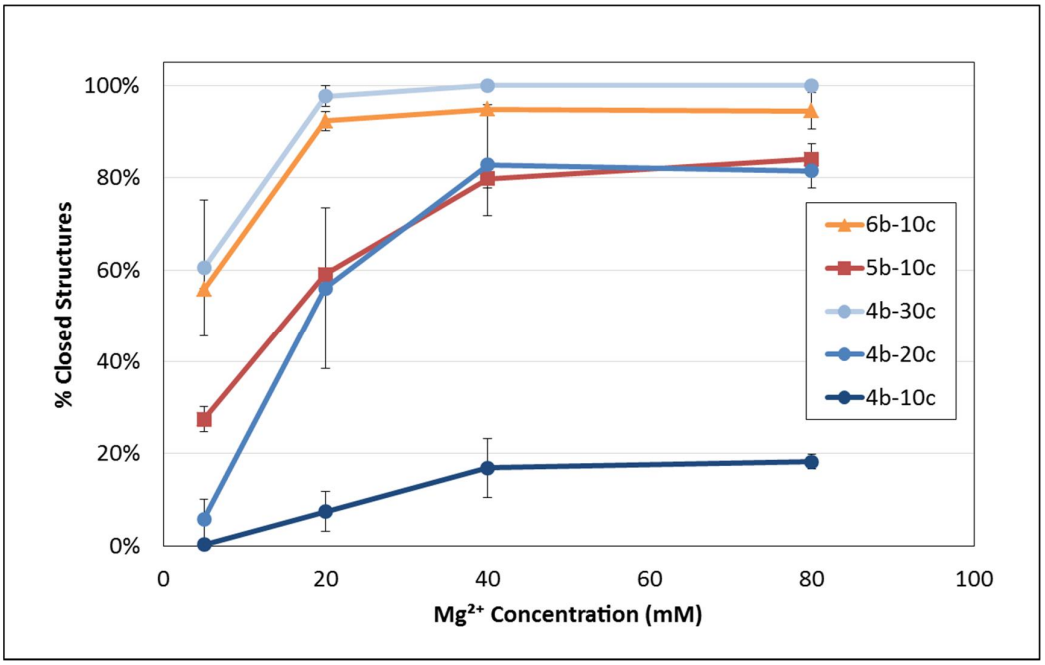

Figure 18: A summary of all H1OH trials shows that hinges close more readily with increasing solution-ion concentration, overhang length, and number of overhang connections.

We concluded that solution ion concentration, overhang length, and number of overhang connections all directly affect hinge actuation. Hinges seemed to have a maximum closing ability for any given overhang configuration. Analyzing the comprehensive plot in Figure 18, it is also interesting to note the curve clustering of a few of the designs. The 5b-10c curve was very similar to the 4b-20c, as was the 6b-10c curve to the 4b-30c curve. Originally, it was thought that each one of these designs would behave independently, which would lead to actuation curves that spanned all different regions of this plot. Instead, though, and as will be discussed in the later section of Hinge 1 with overhangs vs. Hinge 2 with overhangs, we observe an almost quantized partitioning of actuation curves. Initial speculations into why this would be the case have led the group to think that there may exist some energy cost for hinges to close, which can be similarly overcome with a few relatively stronger connections or more relatively weaker connections. Generally these energy barriers to closing could be surmounted as a function of total overhang closing pairs, overhang lengths, number of overhang connections, and location of overhang connections on the hinge arms (also to be discussed in a later sections). This theory finds its foundation in previous studies outlining oligomer thermodynamics. Work in this field suggests that there

exists a specific melting temperature for every Watson-Crick base-pair, and that this melting temperature is directly impacted by base sequence and the "nearest-neighbor" interactions [19].

3.4 Hinge 1 vs. Hinge 2

It has already been established that Hinge 1 is stiffer than Hinge 2, meaning Hinge 2 prefers to be at lower angles. The next HingeOH experiment was based on the hypothesis that basic hinge flexibility effected how readily that hinge would close as solution ion concentration increased. New hinges were designed by adding similar overhangs to Hinge 2 (H2OH), and the same actuation tests were conducted as with H1OH.

Three different H2OH designs were tested: 4b-10c, 4b-20c, and 4b-30c. For each H2OH trial, the structures were folded in 20 mM $MgCl_2$ for a 2.5 day annealing ramp, gel purified, and resuspended in 5 mM, 20 mM, or 40 mM $MgCl_2$ solution; less than three full replicates could be completed for hinges resuspended in 80 mM $MgCl_2$ due to excessive aggregation and poor staining quality, which has forced us to relegate this data to Section 3.6—Additional Trials. TEM images revealed large populations of well-folded hinges that could be counted as either open or closed. A sample size of at least 200 hinges was recorded for each configuration, ion concentration and trial, and three total replicates of each measurement were recorded.

During gel purification of the H2OH 4b-20c structures, an interesting split-band phenomenon was observed in which slower band of structures ran at an expected pace (generally in-line with the blank scaffold band), but a second band of structures appeared to run slightly faster. An example of this split band can be seen in Figure 19. Without an understanding of why this was occurring, structures from each band were extracted, resuspended, imaged and counted independently for all three trials of the 4b-20c tests.

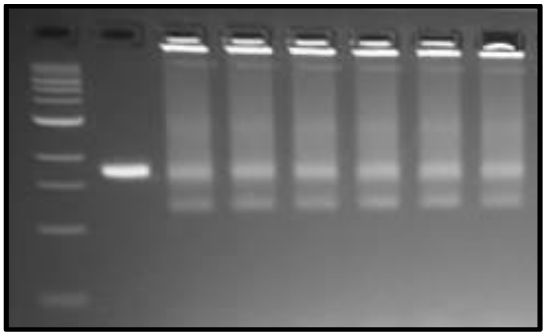

Figure 19: A split band was observed during gel purification of H2OH 4b-20c structures.

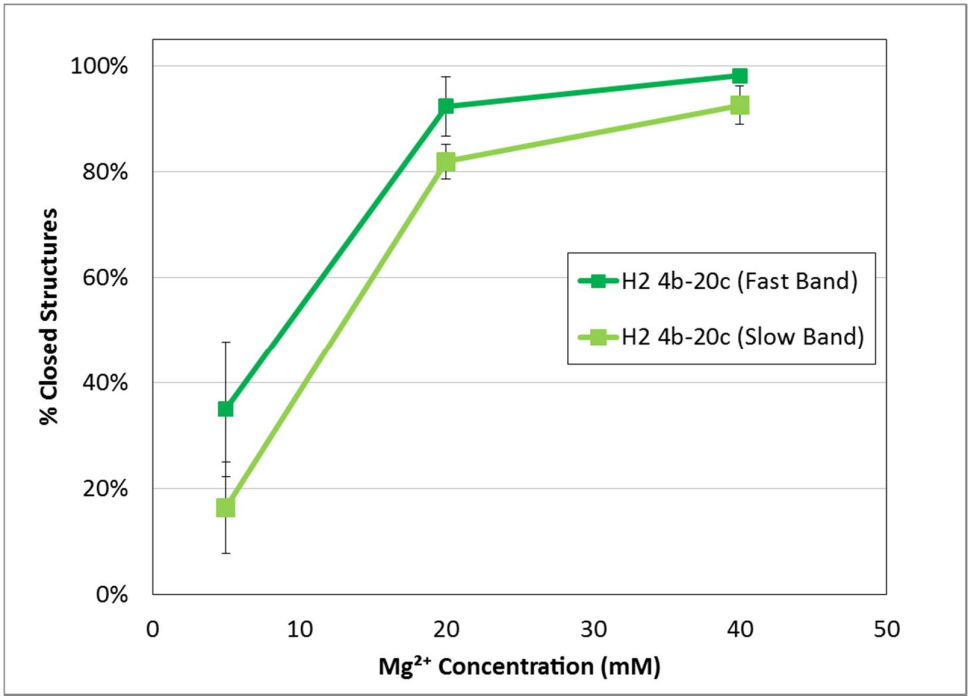

Figure 20: The fast and slow bands were counted independently for all H2OH 4b-20c trials, and resulted in different actuation curves. The fast band consistently closed more than the slow band for at every ion concentration.

Figure 20 displays the actuation curves of the fast and slow bands for the H2OH 4b-20c trials. The split band phenomenon in the gel is supported by the significant difference in closing character of the hinges pulled from the two bands. The fast band produced hinges that closed 5-20% more than the slow band across the ion concentration range. At this time, we cannot definitively explain this split band theoretically, but our current hypothesis is that there is an inhomogeneity in the structures, where a couple staples could have been omitted

during folding. While the omission of these staples would not influence the appearance of the hinges, as could be seen in TEM images, it is possible that structures misfolded without these staples would both run at a slightly slower rate during gel electrophoresis [53] and have slightly different mechanical properties. Since we do not yet definitively understand the split bands, we recorded the closing information from both separately, but then combined the results. The average of percent closed structures was calculated using Equation 4 and used for all further actuation curves.

Equation 4: Average closing percent of split band hinges

$$Average\ \%\ Closed\ Structures = \frac{[N\ closed\ (fast\ band)] + [N\ closed\ (slow\ band)]}{[N\ total\ (fast\ band)] + [N\ total\ (slow\ band)]}$$

Actuation curves were developed in order to visualize the closing of each hinge design across the ion concentration range. In Figure 21 it can be seen that, similar to Hinge 1 with overhangs, actuation increased with increasing solution ion concentration and number of overhang connections. Figure 22 is even more telling of H2OH's actuation character, where when compared with H1OH with the same number of overhang connections and lengths, H2OH closes much more readily than H1OH. This is more than likely due to Hinge 2's lower compared to Hinge 1's. A full comparison of all H1OH and H2OH designs can be found in Figure 23.

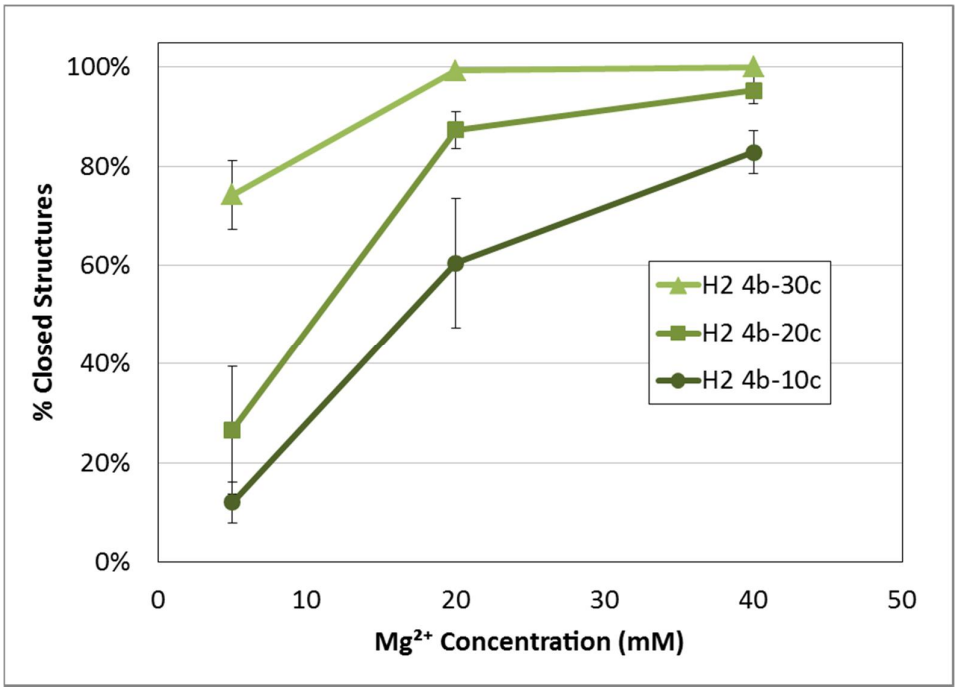

Figure 21: Actuation curves for Hinge 2 with 4-base overhangs and 10, 20, and 30 overhang connections. H2OH closes more readily with increasing number of overhang connections.

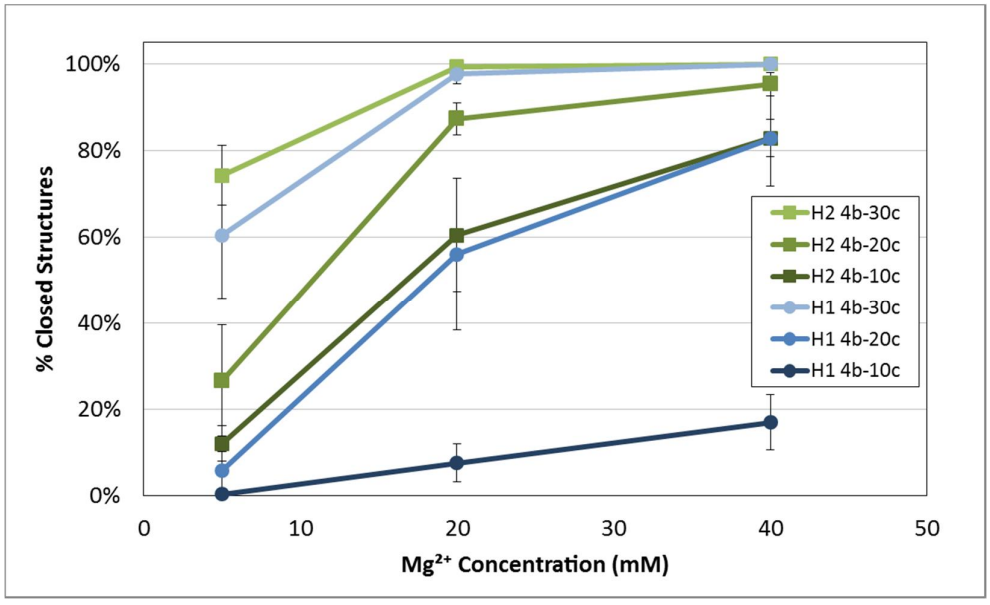

Figure 22: A comparison of H1OH and H2OH shows that Hinge 2 closes more readily than Hinge 1.

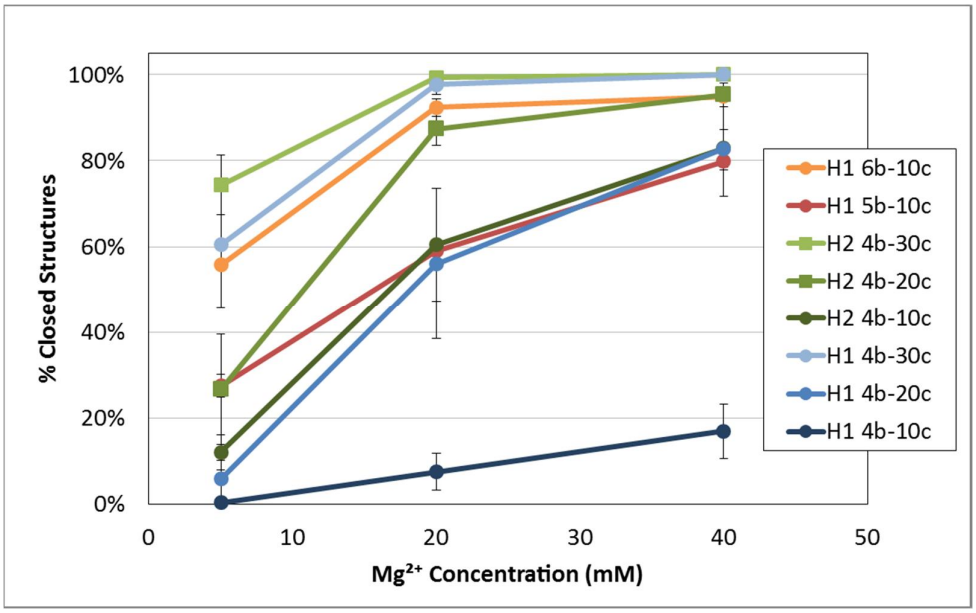

Figure 23: A comprehensive summary of all HingeOH trials shows that hinge actuation can be predictably tuned with overhang length, number of overhangs, and hinge stiffness.

It can be concluded after these trials that the actuation of DNA origami hinges can not only respond predictably to environmental factors such as ion concentration, but also that the actuation of these hinges can be tuned through the modification of design factors like overhang length, number of overhangs, and overall hinge stiffness. The dynamic control over hinge actuation like this could be used in a number of applications, and is a promising step forward in the understanding of how DNA nanostructures can be created to actively change conformations based solely on changing environments.

3.5 Localized Overhangs

After characterizing the effect of number of overhang connections and length of overhangs on the actuation of hinges in an ion-rich solution, a major question left unanswered was whether or not the location of overhangs in reference to the hinge vertex had any effect on closing ability, or if a cluster of overhang acts differently than the same overhangs distributed evenly across the length of the arms. Clustering of overhangs could change the cooperative nature of hinge actuation. We hypothesized that the distance from the vertex of ssDNA overhangs, and clustering of these overhangs, does in fact have an

influence on hinge actuation, and tested this hypothesis through the design of three "localized overhang" hinges.

Hinge 1 was modified by placing 10 overhang connections either near the vertex (H1OH-Near), in the middle of the hinge arms (H1OH-Mid), or at the end of the hinge arms (H1OH-End). These overhangs were each five bases long and all contained the same base sequence as the initial Hinge 1 with 5-base overhangs. The basic design of all three modifications is shown in Figure 24.

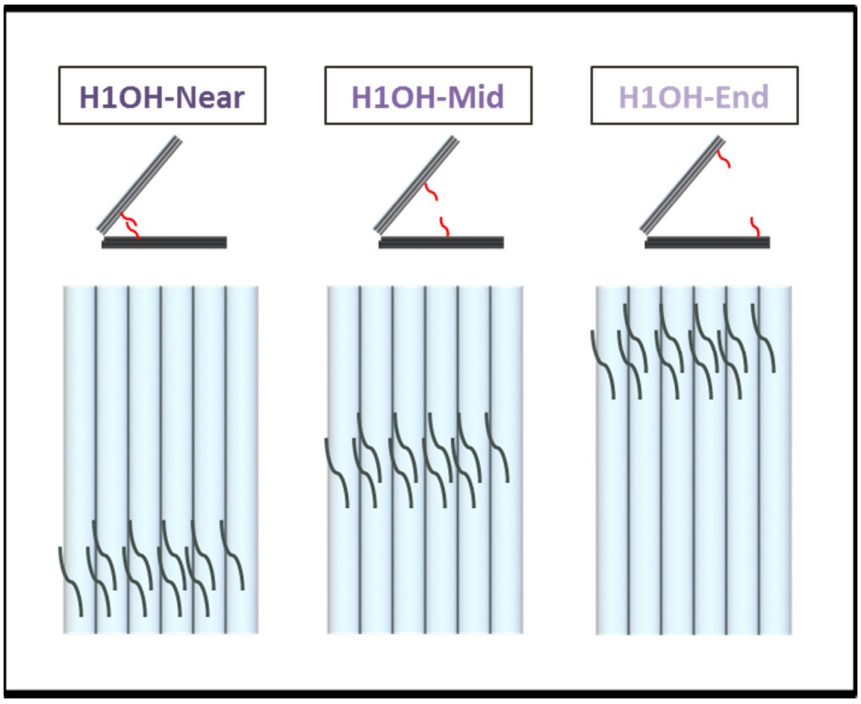

Figure 24: Hinge 1 was modified with 10 overhang connections, each 5 bases longs, clustered near the vertex (H1OH-Near), in the middle of the arm (H1OH-Mid), or at the end of the arm (H1OH-End).

Three different localized H1OH designs were tested: H1 5b10c-Near, H1 5b10c-Mid and H1 5b10c-End. For each localized H1OH trial, the structures were folded in 20 mM $MgCl_2$ for either a 2.5 day annealing ramp or 4 hour rapid fold, gel purified, and resuspended in 5 mM, 20 mM, or 40 mM $MgCl_2$ solution. Just like in trials of previous configurations, TEM images revealed well-folded hinges that exhibited a distribution of open or closed states. A sample size of at least 200 hinges was recorded for each configuration, ion concentration and trial, and two total replicates of each measurement were recorded.

Due to the clustering of overhangs on the inside of the hinge arms, we observed an irregular closing of a small percentage of H1OH-Near and H1OH-Mid hinges where it seemed like the overhangs paired naturally, but the hinge arms bent outwards past the overhang connections causing the hinge to not look completely closed. Examples of this partial closing could be clearly distinguished in TEM images, as can be seen in Figure 25. While these partially-closed hinges exhibited the ssDNA overhang interactions being studied, the hinges were counted separately and excluded from actuation curves so as to avoid future discrepancies in discussing full hinge actuation and overhang interactions. Partially-closed hinges made up no more than 10% of counted hinges for any trial.

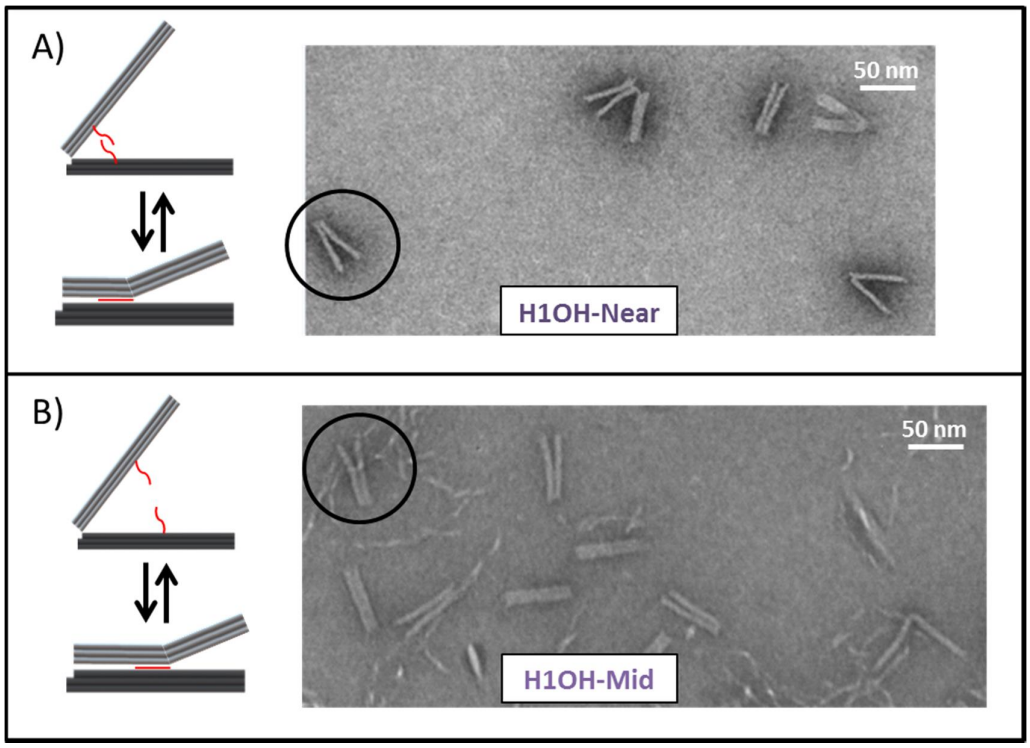

Figure 25: Partial closing was observed in a small percentage of A) H1OH-Near and B) H1OH-Mid hinges.

Split bands were again observed during gel purification, like in H2 4b-20c trials, for H1OH-End and H1OH-Mid hinges. Structures from the fast and slow bands were extracted separately, resuspended, imaged and counted independently for all three trials. As can be seen in Figure 26, hinges extracted from the fast band closed much more readily than hinges from the slow band for both overhang configurations. Six lanes were run of each structure to

show consistency. It is interesting to note that the gap between actuation curves was much wider for these localized configurations (20-50%) than for the H2 4b-20c split band actuation curves (5-20%). It remains unclear why this phenomenon is observed, but trials were continued using an average closing percent of the two bands calculated with Equation 4.

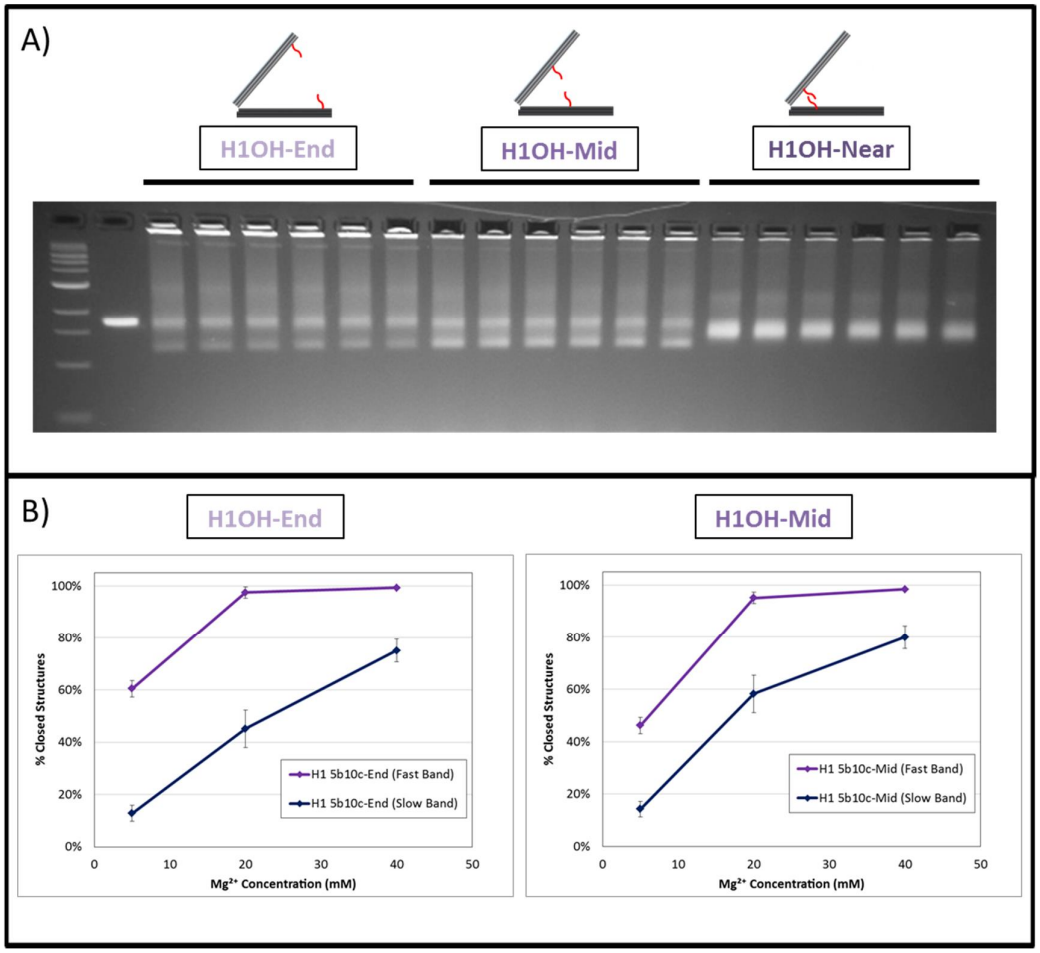

Figure 26: A split band was observed during A) gel purification of H1OH-End and H1OH-Mid hinges. B) Actuation curves of these two configurations were created and show that fast band hinges close much more readily than slow band hinges.

Similar to the previous actuation studies, actuation curves were developed for each overhang configuration in order to visualize differences in closing character. Figure 27 shows that H1 5b10c-End and H1 5b10c-Mid hinges closed much more readily at each solution-ion concentration than H1 5b10c-Near hinges. It is also interesting to note that the H1OH-End

and H1OH-Mid hinges behaved very similarly despite the difference in overhang location being the same as the difference between H1OH-Mid and H1OH-Near overhang locations.

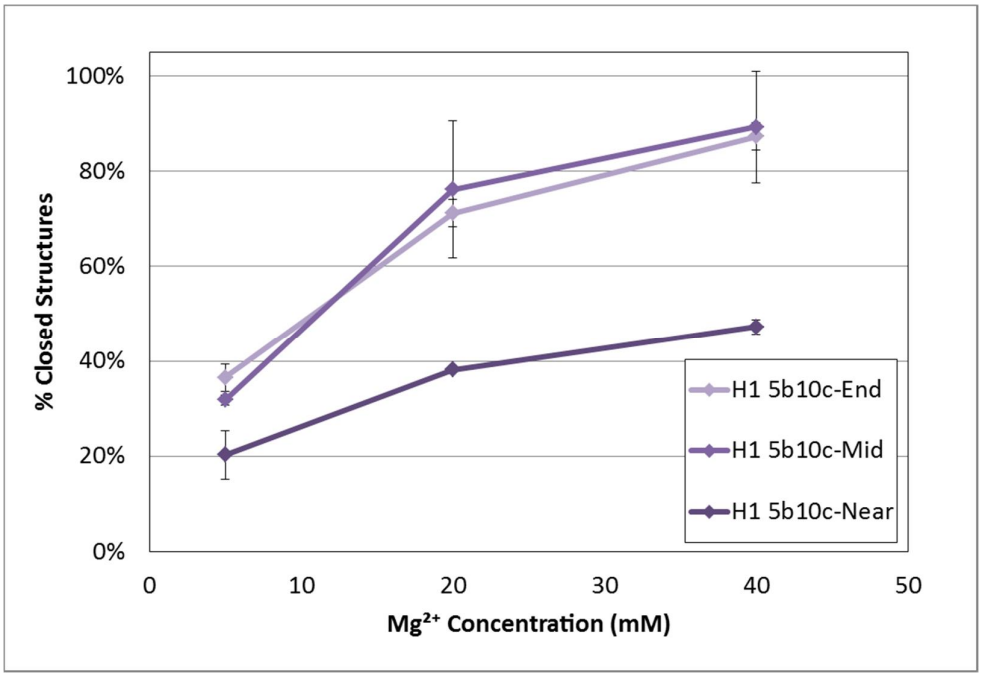

Figure 27: Actuation curves for Hinge 1 localized overhang trials. 5b10c-End and 5b10c-Mid close significantly more than 5b10c-Near at each ion concentration.

Greater insight into the effect of overhang location and clustering can be gained by looking at these localized overhang trials compared to the rest of H1OH trials with 10 overhang connections. This graphic can be found in Figure 28. Hinges with localized overhangs in the middle and at the end of hinge arms closed more readily than hinges with the same amount of overhang connections evenly distributed across both arms, while hinges with localized overhangs near the vertex did not close as readily as hinges with evenly distributed overhangs. This suggests that the actuation character of hinges is directly affected by both the location and clustering of overhangs. In order to explain the effect of overhang location, it could be possible that while the binding energy would be the same, overhangs towards the end of hinge arms have effectively stronger closing capabilities than overhangs closer to the vertex. It is also reasonable to suggest that the clustering of overhangs would close hinges more readily due to the cooperative nature of these interactions. When overhangs are closer together and one binds to the corresponding

overhang on the opposite arm, the adjacent overhangs are automatically brought into much closer proximity to their correspondents and thus are more likely to bind.

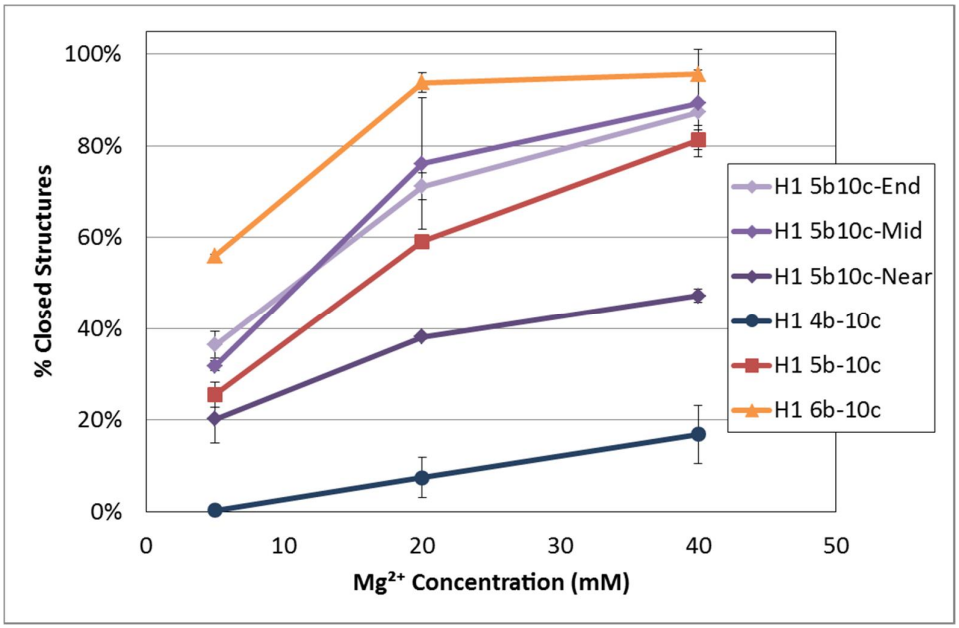

Figure 28: Actuation curves of all H1OH with 10 overhang connections show that localized overhangs in the middle and at the end of hinge arms cause greater actuation than evenly distributed overhangs (H1 5b-10c).

Figure 29 shows a comprehensive summary of all hingeOH conducted for this paper. It is clear that, for every hinge modification, actuation is increased as solution-ion concentration in increased. This is due to the increased stability from cation interactions with negatively-charged DNA molecules. Many hinge design factors also influence actuation. A comparison of several H1OH configurations showed that hinge actuation consistently increased with increasing number of overhang connections and overhang lengths. When H2OH was compared to H1OH with the same number of overhang connections and varying overhang lengths, we observed that H2OH closed more readily than H1OH and concluded that hinge stiffness directly impacts actuation. Finally, the most recently-discussed localized overhang trials show that the location and clustering of overhangs on hinge arms affected actuation as well. We conclude that many design factors can be adjusted to achieve a desired actuation profile in a given solution-ion concentration range.

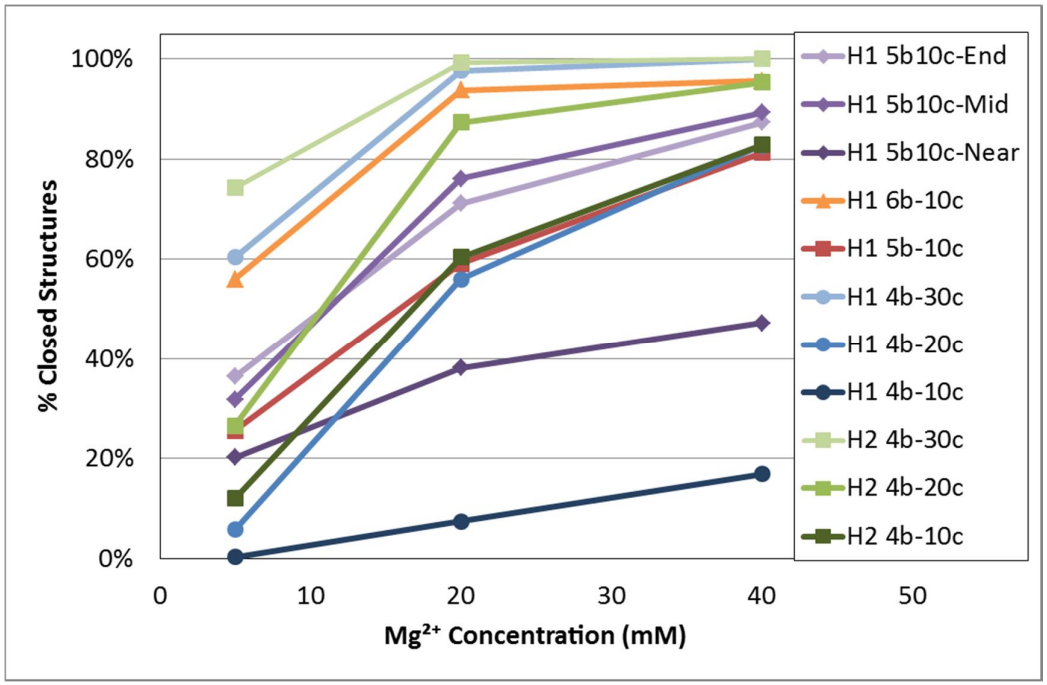

Figure 29: Comprehensive display of actuation curves for every hingeOH trials shows that actuation can be controlled through the tuning of many intrinsic design factors.

3.6 Additional Trials

While the most complete and educational hinge characterization and actuation trials have already been presented, it is important to also note both the trials that were inconclusive and the research that was not seen to completion.

Most notable were the H2OH hinge actuation trials in 80 mM $MgCl_2$, in which two replicate experiments were completed but data was deemed inconclusive due to excessive aggregation of structures, which is common at these ver high salt concentrations. We observed enough structures on the TEM to notice large clumps of structures towards the peripheries of grids for these trials, and the closing percent of hinges for these trials was much lower than expected based on H1OH 80 mM $MgCl_2$ trials conducted previously. Due to the additional complications that come with these high ion concentrations, structures were no longer suspended in 80 mM $MgCl_2$ for the ensuing localized overhang trials.

A smaller study not included in the primary discussion of this paper, due only to the lack experimental replicates, focused on the actuation of Hinge 1 with 25 overhang connections

each 4 bases long (H1 4b-25c). One full trial was conducted, and it is interesting to note that the actuation curve for this configuration was very similar to that of H1 4b-30c, as can be seen in Figure 30.

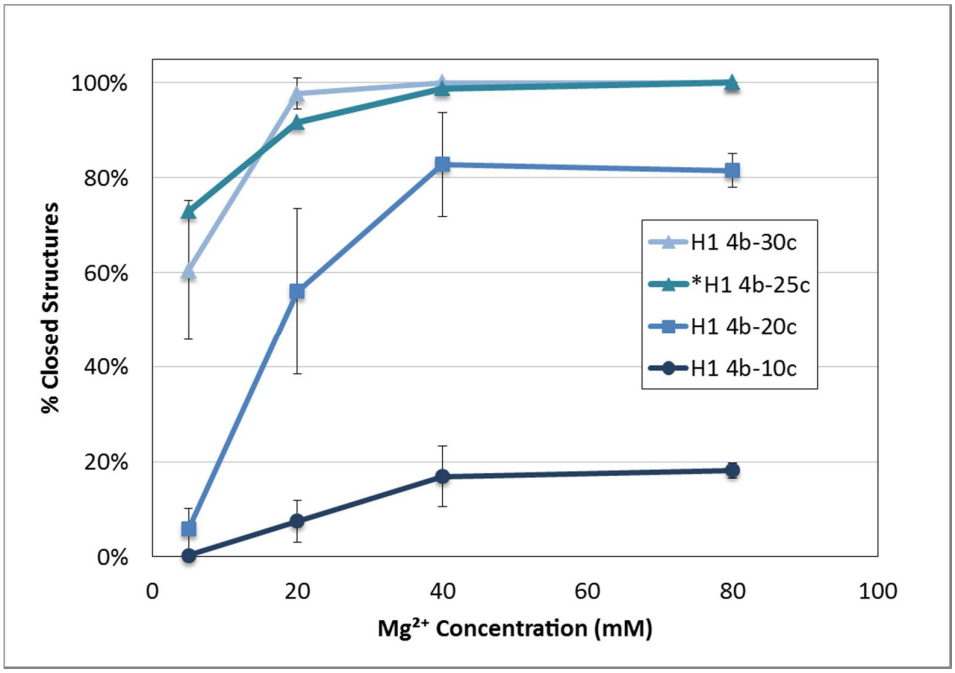

Figure 30: One trial of the H1 4b-25c configuration showed that its actuation curve was similar to H1 4b-30c.

H1OH with 3-base overhangs were created and tested for one trial, but did not show any significant closing character at any solution-ion concentration. Therefore, these trials were ended and the focus was shifted to hinges with greater overhang strength.

Chapter 4: Oscillator Hinge

4.1 Two-way Actuation Design

In the field of nanotechnology, dynamic structures have been somewhat limited in their applications owing to the design complexity necessary for creating mechanical nanodevices. The nanohinge discussed earlier will find many useful applications in drug delivery, molecular manipulation, and biophysical assays, but will be limited by its relatively simple design and actuation capabilities. In order to expand on the functionality of the basic hinge, we sought to design a DNA origami structure that could employ multiple actuation mechanisms.

The preliminary design of the novel oscillator hinge incorporates a long, rigid 16-helix bundle base connected to a rigid, v-shaped 16-helix bundle structure that can oscillate on a single plane. The motion models that of a see-saw, in which as the structure pivots around its vertex, one arm of the "v" moves closer to the base and forces the other arm to move farther from the base. A 4-helix bundle support beam connects the two arms of the "v" in anticipation of strain at this point that could bow out the arms as the oscillator is actuated. A general design, caDNAno model, and TEM image of the oscillator hinge can be found in Figure 31.

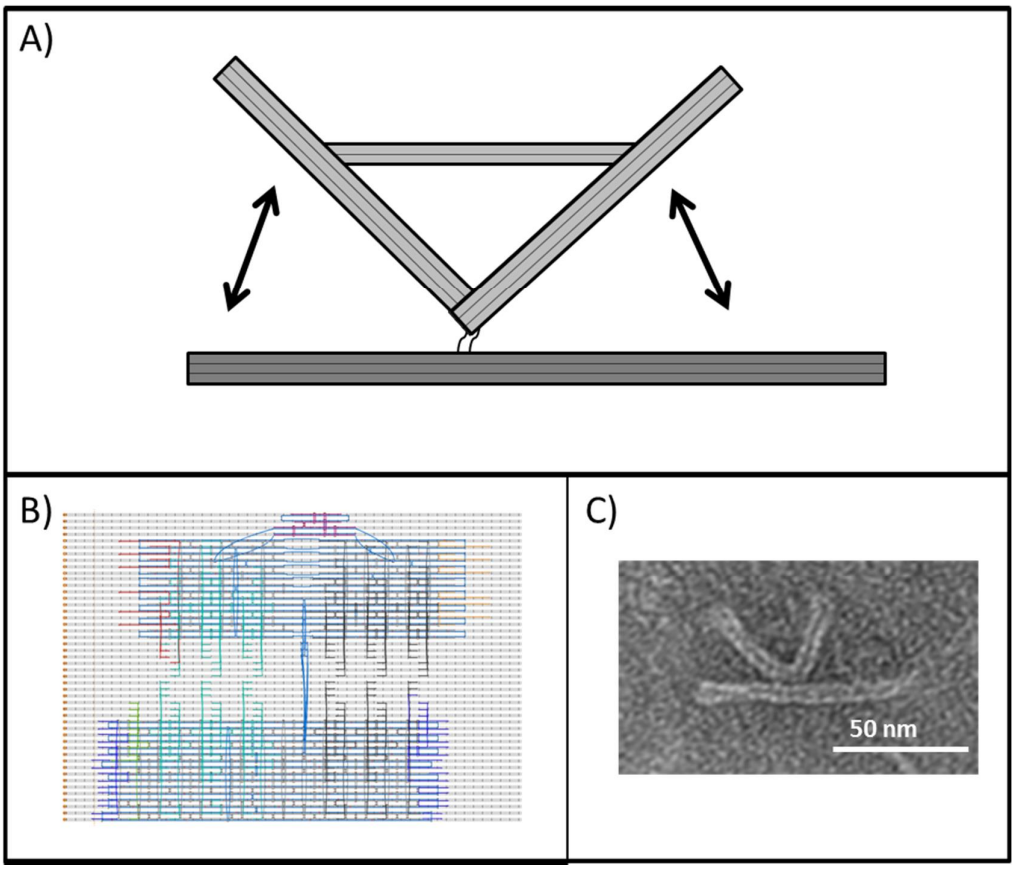

Figure 31: A) The oscillator hinge was designed with a rigid base connected to a v-shaped, rigid dual-arm capable of moving along a single plane on top of the base. B) caDNAno design of the oscillator hinge. C) TEM image of the first successfully fabricated oscillator hinges.

The primary goal in designing the oscillator hinge was to create a nanodevice capable of incorporating two different actuation mechanisms—ion-based actuation and target-based actuation. Ion-based actuation is the mechanism used for all of the previously-discussed hingeOH trials. In this, complementary ssDNA overhangs are added to the inside faces of the hinge that, in the presence of an adequate solution-ion concentration, will bind as Watson-Crick base-pairs and force the hinge closed in that direction. This actuation mechanism has been analyzed in great detail, and allows the user to tune the design of the oscillator hinge based on several overhang factors to close across a wide range of ion concentrations. The second actuation mechanism to be used with the oscillator hinge, target-based actuation, builds off of the strand displacement [43] and low-affinity hinge trials completed in the NBL lab by Alex Marras. For this form of actuation, ssDNA overhangs are incorporated onto the

inside faces of the hinges that are not complementary to each other, but instead are both partially-complementary to a separate target strand of ssDNA (t-ssDNA). In the presence of these free-floating t-ssDNA strands, the hinge overhangs will both bind to part of the strand, forcing the hinge closed in that direction. Preliminary studies with this mechanism suggest that, similar to the positive relationship between ion concentration and ion-based actuation, target-based actuation can be increased through increasing t-ssDNA concentrations. Using target-based actuation allows the user to open hinges through strand displacement, in which ssDNA fully complementary to the t-ssDNA is introduced to the system. This fully-complementary strand will bind to the t-ssDNA, pulling it from the hinge overhangs and thus freeing the hinge to open. A schematic of this mechanism can be found Figure 32.

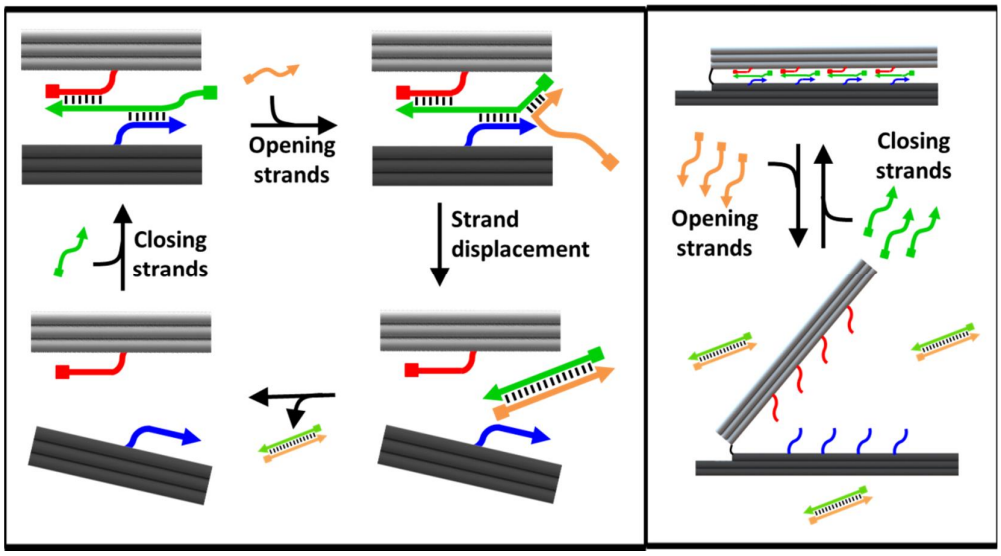

Figure 32: Target-based actuation utilizes uncomplementary overhangs that are partially complementary to a target ssDNA strand. In the presence of the t-ssDNA, hinges will be forced closed, and can be opened again through the introduction of opening strands that are fully complementary to t-ssDNA strands.

Incorporating one actuation method on each side of the oscillator hinge should produce the opportunity to study competing actuation strengths of these methods, and designing an oscillator that can respond to multiple solution-environment factors. Figure 33 shows a schematic displaying the dual-actuation capabilities of the oscillator hinge.

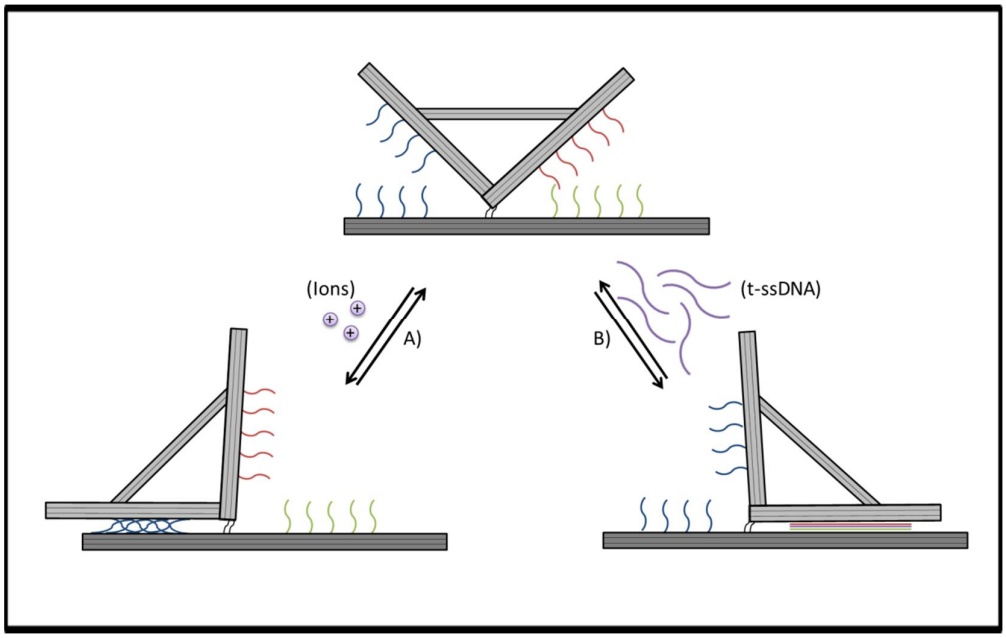

Figure 33: The oscillator hinge can be modified to incorporate two different and competing actuation methods. A) The ion-based actuation mechanism causes complementary overhangs on the hinge to bind in the presence of sufficient solution-ions, causing the hinge to close in that direction. B) Target-based actuation is achieved through incorporating non-complementary overhangs that are both partially-complementary to a target ssDNA strand (t-ssDNA), and bind in the presence of a sufficient concentration of t-ssDNA to close the hinge.

4.2 Desired Applications

The NBL lab plans to use the oscillator hinge for many applications. Of the several directions of work that could be pursued with this design, we will focus on two promising ideas that utilize the oscillator's dual-actuation design for very different reasons—polymerization of oscillator hinges for signal transduction, and dual-actuation for therapeutic and diagnostic (theranostic) employments.

One of the unique properties of DNA origami nanotechnology is the ability to achieve self-assembled, higher-order molecular architectures through programming the polymerization of simple structures [54] [55]. We seek to utilize the programmable self-assembly of many oscillator hinges in order to polymerize a chain capable of propagating a signal through the step-wise actuation of many oscillators. In this mechanism, the oscillator hinges would be modified with overhangs for both actuation methods as well as with a "locking" strand, which will force the hinge closed in one direction until it is unlocked by the

actuation of the adjacent oscillator. A schematic of this theoretical mechanism can be found below in Figure 34.

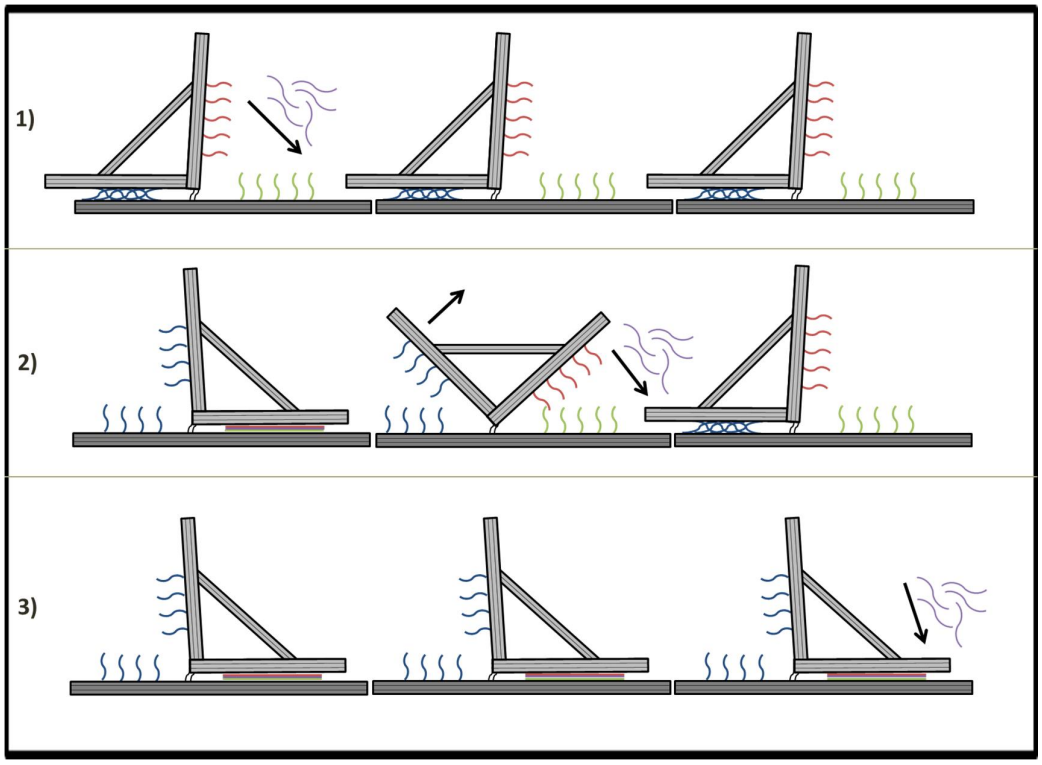

Figure 34: Schematic for the theoretical propagation of a signal through the step-wise actuation of polymerized oscillator hinges.

The oscillator hinge could also be used as theranostic device that both targets a specific gene and treats the disease indicated by that gene. For this application, the oscillator would be modified with overhangs for both actuation methods. The target-based actuation overhangs would be programmed to bind to a gene that is indicative of some disease, so that in the presence of a high concentration of that gene, the oscillator would actuate in that direction. The target-based actuation would force the ion-based overhang bonds to break, opening this side of the hinge that could be functionalized with molecules of disease-specific drugs or fluorescent indicators. One possible application of this theranostic employment could be for the target and treatment of leukemia through the targeting of membrane nucleolin. The aptamer AS1411 has been shown to target nucleolin in leukemia cells [56] and destabilize messenger RNA in cancer cells [57], so incorporating pieces of this aptamer's sequence into the overhangs in the oscillator would possibly create a device that could

target and slow the growth of leukemia cells. Functionalizing the ion-based actuation overhangs with fluorescent molecules would allow the oscillators to exhibit fluorescence when opened through fluorescent resonance energy transfer (FRET) [58]. A schematic of this theoretical theranostic application can be found in Figure 35.

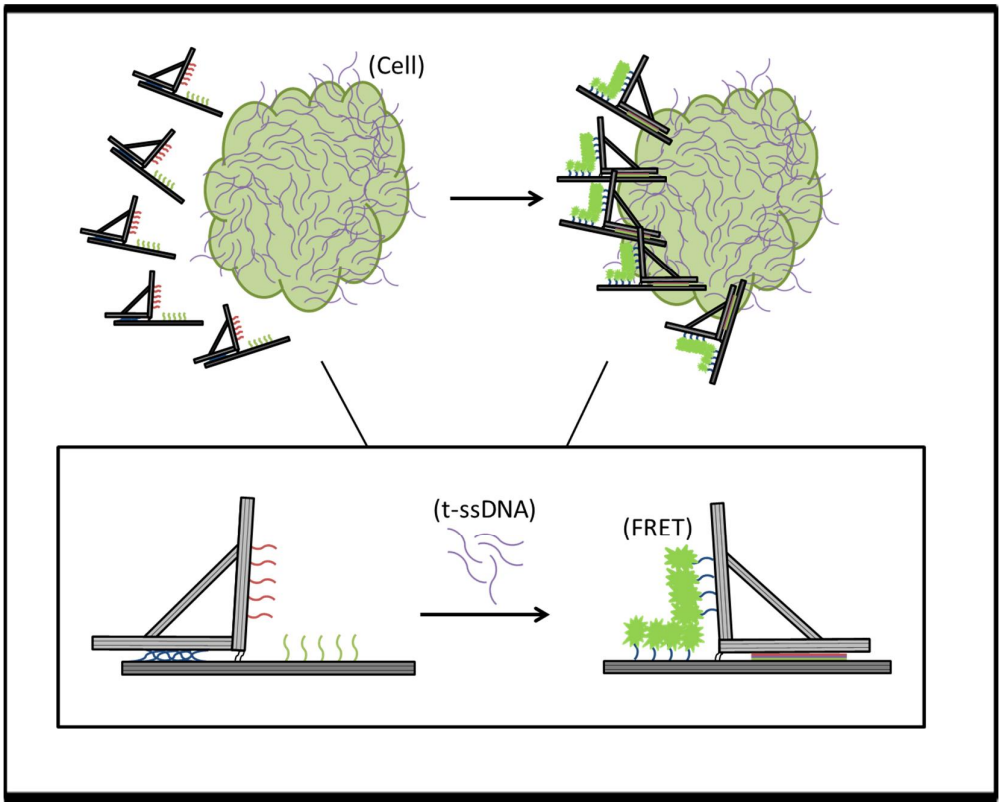

Figure 35: The oscillator hinge could be used as a theranostic device with the incorporation of target-based actuation overhangs to bind to specific cell membrane genes and FRET molecules to exhibit fluorescence. Note—oscillators are not drawn to scale of the cells.

While these applications are merely theoretical currently, they represent the promising future for the novel oscillator hinge. These applications, along with the analysis of competing actuation mechanisms, will be pursued by members of the NBL lab.

Chapter 5: Conclusions and Future Work

5.1 Conclusions

Nanostructures created with scaffolded DNA origami can be used in a variety of applications, including, but not limited to, biosensing, targeted therapies, and mechanical manipulation. The characterization of DNA nanostructure behavior and actuation in common, ion-rich environments is important for the development of dynamic architectures capable of autonomously responding to specific environmental factors. We show that dynamic scaffolded DNA origami hinges can be modified with ssDNA overhangs in order to control conformational changes in a given solution-ion concentration range. Hinge design factors, including hinge stiffness, number of overhang connections, length of overhangs, and location of overhangs, can be tuned to achieve very specific closing character.

We also designed and fabricated a novel oscillator hinge for dual-actuation capabilities. The oscillator hinge can be modified with ssDNA overhangs on both sides and incorporate competing actuation mechanisms—ion-based and target-based actuation.

Characterization of the dynamic nanohinge and preliminary work with the oscillator hinge have provided us with valuable insight into what the future may hold for the applications of reconfigurable DNA nanostructures.

5.2 Future Work

Future experiments will be designed to expand on work with both the hinge and oscillator hinge. The hinge will be modified with overhangs clustered length-wise on each arm to study the actuation strength compared to width-wise clusters. An analysis of real-time actuation of hinges will also be conducted using fluorescent overhangs and a fluorometer. We are also currently collaborating with Dr. Gaurav Arya at University of California San Diego to create adequate models for the estimation of hinge actuation based on design and environment parameters.

Competing actuation mechanism experiments will be performed with the oscillator hinge to understand the relationship between ion-based actuation and target-based actuation. An end goal with the oscillator hinge is to fabricate polymerized chains for signal

propagation, as well as the use as a possible theranostic device. Continued progress with both of these scaffolded DNA origami structures will open the door for innovative applications to address a vast range of medical, material, and scientific needs. In conclusion, the future is bright both in the Nanoengineering and Biodesign Lab and in the field of DNA nanotechnology as a whole.

References

[1] H. Nichols, "The top 10 leading causes of death in the US," 21 September 2015. [Online]. Available: http://www.medicalnewstoday.com/articles/282929.php.

[2] Nanowerk, "Nanotechnology in Energy," 2016. [Online]. Available: http://www.nanowerk.com/nanotechnology-in-energy.php.

[3] United States National Nanotechnology Initiative, "What is Nanotechnology?," 2016. [Online]. Available: http://www.nano.gov/nanotech-101/what/definition.

[4] C. Phoenix, "History of Nanotechnology," 20 April 2015. [Online]. Available: http://www.nanotech-now.com/Press_Kit/nanotechnology-history.htm.

[5] J. R. Kanwar, X. Sun, V. Punj, B. Sriramoju, R. R. Mohan, S.-F. Zhou, A. Chauhan and R. K. Kanwar, "Nanoparticles in the treatment and diagnosis of neurological disorders: untamed dragon with fire power to heal," *Nanomedicine: Nanotechnology, Biology, and Medicine,* pp. 399-414, 2011.

[6] S. Wohlfart, S. Gelperina and J. Kreuter, "Transport of drugs across the blood–brain barrier by nanoparticles," *Journal of Controlled Release,* pp. 264-273, 2012.

[7] S. Parveen, R. Misra and S. K. Sahoo, "Nanoparticles: a boon to drug delivery, therapeutics, diagnostics and imaging," *Nanomedicine: Nanotechnology, Biology, and Medicine,* pp. 147-166, 2012.

[8] D. B. Beach, A. J. Rondinone, B. G. Sumpter, S. D. Labinov and R. K. Richards, "Solid-State Combustion of Metallic Nanoparticles: New Possibilities for an Alternative Energy Carrier," *Journal of Energy Resources Technology,* pp. 29-32, 2007.

[9] J. Weiss, P. Takhistov and D. J. McClements, "Functional material in food nanotechnology," *Journal of Food Science,* pp. 107-116, 2006.

[10] M. Manoharan, "Research on the frontiers of materials science: The impact of nanotechnology on new material development," *Technology in Society,* pp. 401-404, 2008.

[11] A. G. Cattaneo, R. Gornati, E. Sabbioni, M. Chiriva-Internati, E. Cobos, M. R. Jenkins and G. Bernardini, "Nanotechnology and human health: risks and benefits," *Journal of Applied Toxicology,* pp. 730-744, 2010.

[12] S. K. Sahoo, S. Parveen and J. J. Panda, "The present and future of nanotechnology in human health care," *Nanomedicine: Nanotechnology, Biology, and Medicine,* pp. 20-31, 2007.

[13] N. Seeman, "Nucleic Acid Junctions and Lattices," *Journal of Theoretical Biology,* pp. 237-247, 1982.

[14] P. K. Rothemund, "Folding DNA to create nanoscale shapes and patterns," *Nature,* pp. 297-302, 2006.

[15] V. Linko and H. Dietz, "The Enabled State of DNA Nanotechnology," *Current Opinion in Biotechnology,* pp. 555-561, 2013.

[16] D. Yang, M. J. Campolongo, T. N. Nhi Tran, R. C. H. Ruiz, J. Kahn and D. Luo, "Novel DNA materials and their applications," *WIREs Nanomedicine and Nanobiotechnology,* pp. 648-669, 2010.

[17] C. E. Castro, H. J. Su, A. E. Marras, L. Zhou and J. Johnson, "Mechanical design of DNA nanostructures," *Nanoscale,* pp. 5913-5921, 2015.

[18] J. D. Watson and F. C. Crick, "Molecular Structure of Nucleic Acids: A Structure for Deoxyribose Nucleic Acid," *Nature,* pp. 737-738, 1953.

[19] J. SantaLucia Jr., "A unified view of polymer, dumbbell, and oligonucleotide DNA nearest-neighbor thermodynamics," *PNAS,* pp. 1460-1465, 1998.

[20] L. A. Pray, "Discovery of DNA Structure and Function: Watson and Crick," *Nature Education,* 2008.

[21] J. Chen and N. C. Seeman, "Synthesis from DNA of a molecule with the connectivity of a cube," *Letters to Nature,* pp. 631-633, 1991.

[22] S. M. Douglas, I. Bachelet and G. M. Church, "A Logic-Gated Nanorobot for Targeted Transport of Molecular Payloads," *Science,* pp. 831-834, 2012.

[23] Q. Zhang, Q. Jiang and et-al, "DNA Origami as an In Vivo Drug Delivery Vehicle for Cancer Therapy," *ACS Nano,* pp. 6633-6643, 2014.

[24] C. E. Castro, F. Kilchherr, D.-N. Kim, E. L. Shiao, T. Wauer, P. Wortmann, M. Bathe and H. Dietz, "A primer to scaffolded DNA origami," *Nature Methods,* pp. 221-229, 2011.

[25] S. M. Douglas, H. Dietz, T. Liedl, B. Hogberg, F. Graf and W. M. Shih, "Self-assembly of DNA into nanoscale three-dimensional shapes," *Nature,* pp. 414-418, 2009.

[26] H. Dietz, S. M. Douglas and W. M. Shih, "Folding DNA into twisted and curved nanoscale shapes," *Science,* pp. 725-730, 2009.

[27] C. J. Kearney, C. R. Lucas, F. J. O'Brien and C. E. Castro, "DNA Origami: Folded DNA-Nanodevices That Can Direct and Interpret Cell Behavior," *Adv Mater,* pp. 5509-5524, 2016.

[28] M. Endo, Y. Yang and H. Sugiyama, "DNA origami technology for biomaterials applications," *Biomaterials Science,* pp. 347-360, 2013.

[29] R. Schreiber, J. Do, E.-M. Roller, T. Zhang, V. J. Schuller, P. C. Nickels, J. Feldmann and T. Liedl, "Hierarchical assembly of metal nanoparticles, quantum dots and organic dyes using DNA origami scaffolds," *Nature Nanotechnology,* pp. 74-78, 2014.

[30] K. Du, S. H. Ko, G. M. Gallatin, H. P. Yoon, J. A. Liddle and A. J. Berglund, "Quantum dot-DNA origami binding: a single particle, 3D, real-time tracking study," *Chem. Commun.,* pp. 907-909, 2013.

[31] S. M. Douglas, J. J. Chou and W. M. Shih, "DNA-nanotube-induced alignment of membrane proteins for NMR structure determination," *Proc. Natl. Acad. Sci. USA,* pp. 6644-6648, 2007.

[32] D. N. Selmi, R. J. Adamson, H. Attrill, A. D. Goddard, R. C. Gilbert, A. Watts and A. Turberfield, "DNA-templated proetin arrays for single-molecule imaging," *Nano Letters,* pp. 657-660, 2011.

[33] A. Kuzuya and Y. Ohya, "Nanomechanical Molecular Devices made of DNA Origami," *Acounts of Chemical Research,* pp. 1742-1749, 2014.

[34] A. Kuzuya, Y. Sakai, T. Yamakazi, Y. Xu and M. Komiyama, "Nanomechanical DNA Origami "Single-Molecule Beacons" Directly Imaged by Anotmic Force Microscopy," *Nature Communications,* p. 449, 2011.

[35] N. D. Derr, B. S. Goodman, R. Jungmann, A. E. Leschziner, W. M. Shih and S. L. Reck-Peterson, "Tug-of-war in motor protein ensembles revealed with a programmable DNA origami scaffold," *Science,* pp. 662-665, 2012.

[36] M. Langecker, V. Arnaut, T. G. Martin, J. List, S. Renner, M. Mayer, H. Dietz and F. C. Simmel, "Synthetic lipid membrane channels formed by designed DNA nanostructures," *Science,* pp. 932-936, 2012.

[37] W. Liu, H. Zhong, R. Wang and N. C. Seeman, "Crystalline two-dimensional DNA-origami arrays," *Angew. Chem. Int. Edn. Engl.,* pp. 264-267, 2010.

[38] Y. Ke and et al., "Scaffolded DNA origami of a DNA tetrahedron molecular container," *Nano Letters,* pp. 2445-2447, 2009.

[39] T. Liedl, B. Hogberg, J. Tytell, D. E. Ingber and W. M. Shih, "Self-assembly of three-dimensional prestressed tensegrity structures from DNA," *Nature Nanotechnology,* pp. 520-524, 2010.

[40] B. Sacca and et al., "Orthogonal protein decoration of DNA origami," *Angew. Chem. Int. Edn. Engl.,* pp. 9378-9383, 2010.

[41] B. Yurke, A. J. Turberfield, A. P. Mills Jr., F. C. Simmel and J. L. Neumann, "A DNA-fuelled molecular machine made of DNA," *Nature,* pp. 605-608, 2000.

[42] G. J. Lavella, A. D. Jadhav and M. M. Maharbiz, "A synthetic chemomechanical machine driven by ligand-receptor bonding," *Nano Letters,* pp. 4983-4987, 2012.

[43] A. E. Marras, L. Zhou, H.-J. SU and C. E. Castro, "Programmable motion of DNA origami mechanisms," *Proc. Natl. Acad. Sci. U.S.A.,* pp. 713-718, 2015.

[44] I. Saaem and T. H. LaBean, "Overview of DNA origami formolecular self-assembly," *WIREs Nanomed Nanobiotechnol,* pp. 150-162, 2013.

[45] S. M. Douglas, A. H. Marblestone, S. Teerapittayanon, A. Vazquez, G. M. Church and W. M. Shih, "Rapid prototyping of 3D DNA-origami shapes with caDNAno," *Nucleic Acids Research,* pp. 5001-5006, 2009.

[46] Y. Ke, S. M. Douglas, L. Minghui, J. Sharma, A. Cheng, A. Leung, Y. Liu, W. M. Shih and H. Yan, "Multilayer DNA origami packed on a square lattice," *J Am Chem Soc,* pp. 15903-15908, 2009.

[47] K. Pan, D.-N. Kim, F. Zhang, M. R. Adendorff, H. Yan and M. Bathe, "Lattice-free prediction of three-dimensional structure of programmed DNA assemblies," *Nature Communications,* p. 5578, 2014.

[48] E. Stahl, T. G. Martin, F. Praetorius and H. Dietz, "Facile and Scalable Preparation of Pure and Dense DNA Origami Solutions," *Angew. Chem.,* pp. 12949-12954, 2014.

[49] J.-P. J. Sobczak, T. G. Martin, T. Gerling and H. Dietz, "Rapid Folding of DNA into Nanoscale Shapes at Constant Temperature," *Science,* pp. 1458-1461, 2012.

[50] T. G. Martin and H. Dietz, "Magnesium-free self-assembly of multi-layer DNA objects," *Nature Communications,* pp. 1-6, 2012.

[51] J. Hahn, S. F. Wickham, W. M. Shih and S. D. Perrault, "Addressing the Instability of DNA

Nanostructures in Tissue Culture," *ACS Nano,* pp. 8765-8775, 2014.

[52] ATDBio, "DNA duplex stability," 2016. [Online]. Available: http://www.atdbio.com/content/53/DNA-duplex-stability.

[53] K. F. Wagenbauer, C. H. Wachauf and H. Dietz, "Quantifying quality in DNA self-assembly," *Nature Communications,* pp. 1-7, 2014.

[54] Z. Li, M. Liu, L. Wang, J. Nangreave, H. Yan and Y. Liu, "Molecular Behavior of DNA Origami in Higher-Order Self-Assembly," *J. Am. Chem. Soc.,* pp. 13545-13552, 2010.

[55] Y. Yonamine, K. Cervantes-Salguero, K. Minami, I. Kawamata, W. Nakanishi, J. P. Hill, S. Murate and K. Ariga, "Supramolecular 1-D polymerization of DNA origami through a dynamic process at the 2-dimensionally confined air-water interface," *Phys. Chem. Chem. Phys.,* pp. 12576-12581, 2016.

[56] S. Soundararajan and L. Wang, "Plasma Membrance Nucleolin Is a Receptor for the Anticancer Aptamer AS1411 in MV4-11 Leukemia Cells," *Molecular Pharmacology,* pp. 984-991, 2009.

[57] S. Soundararajan, W. Chen and et-al, "The Nucleolin Targeting Aptamer AS1411 Destabalizes Bcl-2 Messenger RNA in Human Breast Cancer Cells," *AACR,* pp. 2358-2365, 2008.

[58] V. V. Didenko, "DNA Probes Using Fluorescence Resonance Energy Transfer (FRET): Designs and Applications," *Biotechniques,* pp. 1106-1121, 2001.